Perilipin membrane-integration determines lipid droplet heterogeneity in differentiating adipocytes

Mario Majchrzak[2], Ozren Stojanović[1], Dalila Ajjaji[3], Kalthoum Ben M'barek[3], Mohyeddine Omrane[3], Abdou Rachid Thiam[3], Robin W. Klemm[1,2,4,5]

[1]Department of Physiology Anatomy and Genetics, University of Oxford, Oxford OX1 3PT, UK
[2]Department of Molecular Life Sciences, University of Zurich, 8057 Zurich, CH
[3] Laboratoire de Physique de l'École Normale Supérieure, ENS, Université PSL, CNRS, Sorbonne Université, Université de Paris, F-75005 Paris, France
[4]Correspondence : Robin.Klemm@dpag.ox.ac.uk
[5]Lead contact

Summary

The storage of fat within lipid droplets (LDs) of adipocytes is critical for whole-body health. Acute fatty acid (FA) uptake by differentiating adipocytes leads to the formation of at least two LD-classes marked by distinct perilipins (PLINs). How this LD-heterogeneity arises is an important yet unresolved cell biological problem. Here, we show that an unconventional integral membrane-segment (iMS) targets the adipocyte specific LD-surface factor PLIN1 to the endoplasmic reticulum (ER) and facilitates high affinity binding to the first LD-class. The other PLINs remain largely excluded from these LDs until FA-influx recruits them to a second LD-population. Preventing ER-targeting turns PLIN1 into a soluble, cytoplasmic LD-protein, reduces its LD-affinity and switches its LD-class specificity. Conversely, moving the iMS to PLIN2 leads to ER-insertion and formation of a separate LD-class. Our results shed light on how differences in organelle targeting and disparities in lipid-affinity of LD-surface factors contribute to formation of LD-heterogeneity.

Keywords: LD-heterogeneity, LD-targeting, ERTOLD, CYTOLD, LD-affinity, PLIN1

Highlights

- PLIN1 is an integral membrane protein behaving as a class I LD protein.
- An unconventional integral membrane segment (iMS) mediates ER insertion.
- The iMS is required for LD-heterogeneity in differentiating adipocytes.
- High affinity LD-targeting from the ER is likely a gated process.

eTOC blurb

Majchrzak et al. use biochemistry, imaging and *in vitro* experiments to identify molecular features in PLIN1 that determine ER insertion and high lipid droplet affinity which are both important in the generation of LD-heterogeneity within differentiating adipocytes.

Introduction

Adipocytes deposit an excess of dietary nutrients as triacylglycerols (TAGs) in large lipid droplets (LDs) and release fatty acids to feed other tissues during fasting[1–3]. Deficiencies in LD biogenesis and turnover are associated with several metabolic diseases such as lipodystrophies, fatty liver disease, type-2 diabetes, and obesity[4–6].

LDs form at the membranes of the endoplasmic reticulum (ER) when neutral lipids, such as TAGs, accumulate between the two leaflets of the lipid bilayer[7–9]. When TAG-amounts increase they phase-separate and form lenses, which eventually bud out into the cytoplasm as LDs. The LD-surface is surrounded by a phospholipid monolayer and specific surface proteins[10–15].

In principle all LDs within a cell should have the same lipid and protein composition. Accumulating evidence suggests, however, that LDs are highly heterogenous, and can specialize into different sub-populations which are morphologically, chemically, and functionally distinct[14,16–22].

One way by which cells can generate different LD-classes is through the synthesis of the hydrophobic core. For example, fly fat bodies contain a population of large LDs, which is mostly filled with TAGs derived from *de novo* lipogenesis[23,24]. A class of smaller LDs in the periphery of the cell seems to store TAGs made preferentially from dietary fatty acids (FAs)[23,24]. Consistent with these findings, FA feeding of mammalian adipocytes leads to the formation of distinct LD-classes[10,25,26]. A central LD population is formed mainly by *de novo* lipogenesis[27], whereas acute FA influx triggers the formation of a second, peripheral LD class[10,25,26]. The mechanisms that lead to the formation of different LD populations remain, however, poorly understood, and it is largely unclear how LD-surface factors can be targeted to separate LD-populations in the cell.

In general, protein targeting to LDs occurs by two major pathways[14,28,29]. Class I proteins are synthesized as monotopic integral membrane proteins at the ER, and subsequently move to the LD surface using the ERTOLD pathway (**Fig. 1A**, class I). The dual localization to the ER and the LDs is facilitated by special membrane anchors that often fold into hairpins[13,29].
Class II (or CYTOLD) proteins, on the other hand, bind LDs directly from the cytoplasm (**Fig. 1A,** class II). They do not possess integral membrane segments and are instead targeted to the LD by amphipathic domains detecting packing defects in the LD monolayer where the hydrophobic LD core is exposed[14,30–35].

The perilipins (PLINs) are currently viewed as prototypical class II proteins, comprising a family of evolutionarily conserved LD-surface factors carrying out important structural and regulatory functions[26,36–39]. The family defining amphipathic PAT domain and the following 11-mers mediate LD-targeting (**Fig. S1A**)[32,37,40,41]. The PLINs are all thought to target the LD from the cytoplasm and should therefore mix on the same LD class. The LD sub-populations that form in differentiating adipocytes upon FA feeding are, however, marked by specific PLINs (**Fig. 1B**) [10,25,26]. An affinity-based LD binding "hierarchy" among the different PLIN-family members is likely key to the formation of the two LD classes[34,40,42–45]. However, the biochemical characterization of the responsible targeting domains remains incomplete[38].

Results

Acute fatty acid feeding induces the formation of distinct LDs in adipocytes

To investigate perilipin (PLIN) targeting to LDs we differentiated 3T3-L1 cells into white adipocytes and imaged endogenously expressed PLIN1, 2, 3, and 4 after FA feeding (PLIN5 is not expressed in 3T3-L1 adipocytes [11,27]). Confirming previous observations[26,36,39,40,42], we observed distinct LD populations (**Fig. 1B-F**). A central LD class was almost exclusively labelled with PLIN1, and a second, peripheral population was marked by PLIN2, 3, and 4 (Fig. 1C, D, and E). The second population was either exclusively marked by PLIN2, 3, and 4, or contained sometimes low amounts of PLIN1 which we called mixed LDs (**Fig. 1C-E** (zoom-ins), **F** (MIX)).

Consistent with our results in adipocytes and the established LD binding hierarchy[26,43], we next showed that ectopically expressed PLIN1 excluded PLIN2, 3, or 4 from LDs when co-transfected in COS7 cells (**Fig. S1A-D**). This behaviour was dependent on features C-terminally of the 11-mer domain (**Fig. S1A**). A construct only consisting of the N-terminal PAT and 11-mer regions (PLIN1 1-192) mixed well with PLIN2 on the LD surface (**Fig. S1E**).

Together, these data raised the question of how class-II LD proteins can separate onto different LD-populations.

PLIN1 is an integral membrane protein dually localizing to the ER and LDs

To determine the molecular basis of PLIN LD targeting, we expressed PLIN1 and 2 in COS7 cells. As expected, PLIN1 localized to the endogenous LDs but was, surprisingly, never seen in the cytoplasm. Instead, it always bound to the ER (**Fig. 2A, Fig. S2B**). Consistent with previous work[45], these data indicated that PLIN1 is not a prototypical class-II LD protein. On the other hand, PLIN2, showed normal class-II behaviour accumulating in the cytoplasm upon overexpression and covering all endogenous LDs (**Fig. 2B, S2A, S2D**). After addition of FA (Na^+ oleate), both PLIN1 and PLIN2 targeted efficiently to LDs (**Fig. 2C - E**).

Since PLIN1 does not contain any predicted membrane segments (**Fig. S2D, S2E**), and exhibits similar overall hydrophobicity as PLIN2 (**Fig. S2F, S2G**), we initially expected it to bind the ER as a peripheral membrane protein perhaps through a receptor. In support of this view, PLIN1 sedimented together with the endogenously expressed integral ER protein calnexin (CNX) to the membrane pellet (**Fig. 2F**, PLIN1 untagged; GFP-PLIN1, P100).

However, when we subjected the membrane pellet (P100) to alkaline extraction with Na_2CO_3-buffer, PLIN1 remained in the alkaline resistant membrane fraction (**Fig. 2F**, P100E) behaving like an integral membrane protein. PLIN2 co-fractionated with the soluble cytoplasmic marker glyceraldehyde-3-phosphate dehydrogenase (GAPDH, **Fig. 2F**, S100).

To exclude possible artefacts, we carried out flotation experiments with a ribosome stripped membrane fraction from cells expressing PLIN1. **Fig. 2G** shows that PLIN1 moved efficiently out of the bottom fraction and floated on a sucrose step gradient together with ER membranes marked by CNX (5-35% sucrose interface). Addition of detergent to P100 prevented

129 flotation (**Fig. 2H**), and PLIN1 and CNX both remained soluble when we mixed the cell lysate with
130 detergent before high-speed centrifugation (**Fig. 2I**).
131 Taken together, our data indicated that PLIN1 does not belong to the cytoplasmic class-II
132 proteins. As an integral membrane proteins LD-targeting might move from the ER to the LD
133 surface. Indeed, we found that PLIN1 ER-pool re-distributed efficiently to LDs when we blocked
134 translation with cycloheximide 1h before LD induction by FA feeding (**Fig. S2H-J**).
135

136 **PLIN1 contains an unconventional integral membrane segment and a peripheral membrane**
137 **binding motif**

138 We next aimed at identifying the domains necessary for PLIN1 membrane-integration.
139 We, therefore, carried out a systematic structure-function analysis using fluorescence
140 microscopy and subcellular fractionation followed by alkaline extraction as parallel readouts.
141 We started with a minimal N-terminus of the mouse PLIN1 sequence (PLIN1 1-192)
142 containing the PAT and 11-mer regions which are sufficient for LD targeting (**Fig. S3A**)[32,40,43]. As
143 expected, neither of these two domains nor a polybasic region enriched in prolines downstream
144 of the 11-mer region was involved in ER targeting. The N-terminal PLIN1 portion until position
145 237 remained completely soluble (**Fig. 3A**, S100) localizing to the cytoplasm and the endogenous
146 LDs (**Fig. 3B, S3B**).
147 However, a construct extended until residue 281 (PLIN1 1-281) pelleted efficiently to the
148 membrane fraction, was alkaline resistant (**Fig. 3A**, P100E), and localized to the ER as determined
149 by microscopy, indicating that the region between residues 238 and 280 contained an integral
150 membrane segment (iMS) (**Fig. 3A** green domain, and **S3B**). Interestingly, the corresponding C-
151 terminal portion (PLIN1 281-517) was found in the supernatant S100 (**Fig. 3A**) but localized to the
152 ER as shown by microscopy (**Fig. 3D**), suggesting that PLIN1 contains an additional peripheral
153 membrane segment (pMS) contributing to ER-binding. Computational analysis of the C-terminal
154 portion predicted a strong amphipathic region between residues 380 and 400 (**Fig. 3A**, yellow).
155 However, a construct containing this motif (Plin1 371-517) remained completely soluble (**Fig. 3A,**
156 **and 3E**). Further extension of the C-terminal part until the beginning of the 4-helix bundle (PLIN1
157 328-517) led to ER localization (**Fig. 3F**), but this construct remained soluble in the fractionation
158 experiments (**Fig. 3A**), indicating that the potential pMS is positioned in this section of the middle
159 domain (**Fig. 3A**, orange).
160 To narrow down the two membrane binding regions further, we turned to hydropathy
161 plot analysis (**Fig. S2F**). A first segment with moderate hydrophobicity was found between
162 tryptophan 238 and proline 280 of the mouse PLIN1 sequence, corresponding to the region in
163 which we identified the iMS (**Fig. S2F and 3G**). A second slightly hydrophobic region between
164 residues 348 and 370 overlapped with the pMS (**Fig. S2F and 3G**).
165

166 To test the function of these domains in ER targeting we deleted them. PLIN1ΔΔ lacking
167 both the iMS and the pMS (**Fig. 3G**, PLIN1 Δ238-280, Δ348-370) was completely soluble, and did
168 not float (**Fig. 3H**). Additionally, this mutant localized to the cytoplasm (**Fig. 3I**). Although having
169 lost its ability to bind the ER, PLIN1ΔΔ was still found on LDs after FA feeding, and now often
170 mixed with PLIN2 (**Fig. 3J**). In conclusion, removal of the iMS and the pMS converted PLIN1 into
171 a class II LD-protein, targeting LDs directly from the cytoplasm (**Fig. 3K**).

172
173 In agreement with this model, addition of the iMS to PLIN2, right downstream of the 11-
174 mer region (PLIN2-iMS (insertion at position 251)), was sufficient for membrane integration (**Fig**
175 **S3C, S3D, S3E**). ER-insertion of PLIN2-iMS permitted efficient competition with PLIN1 for LD
176 formation at the ER (**Fig. S3E**). However, in contrast to our expectation PLIN2-iMS did not mix
177 with PLIN1 on the same LDs, but tended to segregate onto a separate LD class (**Fig. S3E**),
178 indicating a critical function for the iMS in the nucleation of different LD populations at the ER.
179
180 Taken together our data show that PLIN1 behaves as an integral ER membrane protein
181 showing characteristics of a class-I rather than a class-II LD-protein. Both the iMS and the pMS
182 are sufficient for ER targeting, but membrane integration, and the generation of different LD-
183 classes depend on the iMS. Removing the ability to integrate into the ER converts PLIN1 into a
184 conventional class II LD-protein. The ER-binding deficient PLIN1-mutant mixes better with class
185 II-PLINs on the same LDs indicating that it has reduced LD affinity.
186
187
188 **The iMS is critical in determining PLIN1 LD-binding kinetics**

189 To investigate this possibility, we analysed the monolayer affinity of PLIN1 and PLIN1ΔΔ
190 *in vitro* (**Fig. 4A**,[31]). Shrinkage of the aqueous compartments in a buffer-in-oil system leads to
191 compression of an artificial LD-monolayer at the oil-buffer interface. The proteins fall off the
192 monolayer with progressive reduction of the interface area and accumulate proportionally to
193 their off-rates in the buffer compartment[31]. In agreement with the microscopy and fractionation
194 experiments (**Fig. 3G-K**, and [40,42]), full-length PLIN1 remained efficiently bound to the interface
195 of the buffer compartment, indicating that the high LD affinity is determined by low off-rates
196 from the monolayer (**Fig. 4, B**). In comparison, PLIN1ΔΔ was readily released from the interface,
197 showing faster off-rates and thus lower affinity (**Fig. 4A, B**). The progressive accumulation in the
198 buffer phase showed that PLIN1 excluded PLIN1ΔΔ from the LD surface mimic, confirming the
199 results in cells (**Fig. 4A, B**).
200 To gain insights into the corresponding on-reaction of the binding equilibrium, we used
201 fluorescence recovery after photobleaching. Deletion of either the iMS (PLIN1ΔiMS) alone or
202 together with the pMS (PLIN1ΔΔ) made recovery on the LD faster by more than an order of
203 magnitude compared to a mutant in which the iMS is present and only the pMS is removed
204 (PLIN1ΔpMS) (**Fig. 4C**, still frames in **Fig. S4A**).
205 Together these results suggest that PLIN1 binds LDs with low off and on rates, which is
206 determined by the iMS. LD-binding via the classical amphipathic segments appears to be faster
207 but shows lower LD-affinity.
208 These data suggested that differences in membrane targeting and LD-affinity by the PLINs
209 may provide part of the mechanisms by LD-heterogeneity arises in adipocytes: PLIN1 is targeted
210 to the ER via the iMS where it binds to the emerging LDs with high affinity excluding the low-
211 affinity PLINs. However, because PLIN1 is kinetically trapped on this first LD population it cannot
212 immediately bind to the second LD-class which emerges upon FA feeding. At this stage PLIN2, 3
213 and 4 are can readily bind to the surface of the acutely synthesized LDs from the cytoplasm.
214 Despite their lower LD-affinity, the class-II PLINs label the second LD-population first.

215
216 **Perturbation of PLIN1 membrane targeting leads to a LD-class switch in adipocytes**

217 To test these interpretations directly in adipocytes, we stably integrated GFP-PLIN1 and
218 GFP-PLIN1ΔΔ as inducible transgenes into 3T3L1-preadipocytes. Consistent with the results
219 above, PLIN1ΔΔ was soluble (**Fig. 4D**), and full-length PLIN1 behaved like an integral membrane
220 protein (**Fig. 4D and 4E**). PLIN1 localized to LDs after FA feeding and as in COS7 cells moved from
221 the ER to LDs even when translation was shut off with cycloheximide before LD induction (**Fig.**
222 **S4B-E**).
223
224 After expression of the transgene in day 6 adipocytes, PLIN1ΔΔ behaved like a class-II LD
225 protein being largely excluded from the big LDs which formed during differentiation (**Fig. 4E and**
226 **F**). Endogenous full-length PLIN1 was expressed and floated with the LDs to the top fraction (**Fig.**
227 **4G**). PLIN1ΔΔ, was additionally found in the soluble middle fraction, confirming the microscopy
228 experiments (**Fig. 4E and F**). Although being effectively excluded from the LDs covered by
229 endogenous PLIN1 in cells, PLIN1ΔΔ remains LD binding competent (**Fig. 3J, Fig. 4A**), and likely
230 gets access to TAGs when LDs break during mechanical cell-lysis (**Fig. 4G**).
231
232 Importantly, PLIN1ΔΔ efficiently moved from the cytoplasm to the peripheral LD
233 population which forms after FA feeding (**Fig. 4H and F**). Consistent with the results shown for
234 PLIN2-4 in **Fig. 1**, PLIN1ΔΔ remained largely excluded from the LDs that were covered by
235 endogenously expressed full-length PLIN1 (**Fig. 4H and F**).
236
237 Taken together, these data suggest that removing the iMS and pMS not only reduced LD
238 affinity and turned PLIN1ΔΔ into a class-II LD-protein, but also leads to a change in LD-class
239 specificity (**Fig. S4F**).
240
241 Finally, we examined the localization of endogenously expressed PLIN1 during adipocyte
242 differentiation. As expected, in day 6 adipocytes, PLIN1 localized almost exclusively to the surface
243 of LDs (**Fig. 4I**). However, at earlier time-points, e.g. day 3, endogenous PLIN1 also abundantly
244 present on the peripheral ER (**Fig. 4J** and [10,44,45]), and was completely alkaline-resistant confirming
245 its membrane integration (**Fig. 4L)**. At this stage of differentiation, PLIN1 is probably stock-piled
246 in the ER facilitating rapid expansion of the LD-surface.
247
248 Interestingly, when we triggered the breakdown of the LDs by activating lipolysis, PLIN1
249 efficiently moved at these stages back to the ER (**Fig. 4K-L**). The movement between LDs and the
250 ER was further supported by flotation experiments, showing that stimulation of lipolysis re-
251 distributed PLIN1 away from the remaining floating LDs into the membrane pellet (**Fig. 4M**).
252
253
254
255
256

Discussion

Here, we have shown that contrary to its previous classification PLIN1 behaves as an integral membrane protein and is not classical class-II LD protein. We reveal that an unconventional integral membrane segment (iMS) likely folding as a hairpin is necessary and sufficient for integration into the ER membrane and facilitates high affinity binding to the LD.

PLIN1 moves onto the LDs as soon as they appear during adipocyte differentiation. Due to its high affinity, it excludes the other PLINs from these LDs already at earliest stages in the biosynthesis process. Up until differentiation day 3 the ER and LD pools readily exchange. However, at later stages (starting from day 6), PLIN1 is kinetically "trapped" on the surface of the first LD-class. As a result, the second LD-class which emerges upon FA feeding gets covered by PLIN2-4 which are class-II PLINs targeting the second LD-population from the cytoplasm.

Although we show with translation shut-off experiments that PLIN1 moves from the ER to the LD surface, it remains to be determined whether PLIN1 uses the conventional ERTOLD pathway (**Fig. S4F, ER→LD)**. The length of the iMS of around 30 amino acids (**Fig. S4G**) fits the size of known hairpin motifs, but the iMS exhibits surprisingly low hydrophobicity and does, therefore, not satisfy the basic definition of a conventional ER membrane anchor[46–48]. The iMS contains some features that are also found in other hairpins that move between the ER and the LDs[13], such as prolines and large tryptophanes at the centre of the motif (**Fig. S4G**). Additionally, the iMS is flanked by positively charged residues (**Fig. S4G**)[13], perhaps ensuring the correct membrane topology or contributing to the regulation of LD access and stability on the LD surface.

Consistent with other work[49] our data indicate that the iMS favours the LD surface over the ER bilayer likely explaining why in adipocytes the ER pool is minimal at steady state. Since PLIN1 targets LDs early during biogenesis, it probably enters through the Seipin complex[28,50], but may later on perhaps switch to the bridge pathway that was recently identified[51] in fly, bearing molecular similarity with ER-LD contact sites previously identified in 3T3-L1 cells[52]. Our alkaline extraction data and detailed structure function seem incompatible with a cytoplasmic targeting pathway (**Fig. S4F ER→cytoplasm→LD**), but do not fully exclude this possibility.

The PLIN1 covered LDs are essential for adipose tissue function: Loss of PLIN1 in mice and humans can cause lipodystrophy[4,53] because increased basal adipose lipolysis prevents the efficient LDs expansion[54,55]. The affected patients are highly insulin-resistant and suffer from hypertriglyceridemia, cardiovascular problems and fatty liver disease[55,56]. Partial loss of PLIN1 or PLIN1 haploinsufficiency can, surprisingly, have beneficial effects on metabolic health[57]. According to recent reports some PLIN1 mutants in fact improve metabolic profiles and reduce risk for cardiovascular disease[58,59]. A controlled perturbation of PLIN1 membrane targeting might therefore open avenues for mechanism-based therapy of fatty liver disease, type-2 diabetes, and obesity.

298 **Limitations of this study**

299 A limitation of our study is that adipocyte differentiation in tissue culture may not fully
300 recapitulate real tissue. Future work will address the physiological function of the two LD-classes
301 that form in tissue culture.

302 Another open question is how PLIN1 is targeted to the ER. The simplest model involves
303 membrane-integration by Sec61[60]. However, since the hydrophobicity of the iMS is relatively low,
304 the pathway may depend the endoplasmic reticulum membrane complex (EMC) or requires a
305 chaperone such as GET3/TRC40[61]. It is further still a possibility that in adipocytes PLIN1 is first
306 inserted into the LD surface and then moves to the ER. However, if this were true, the acutely
307 forming smaller LDs would then be covered by PLIN1 and not by different PLIN-family members.

308 Lastly, it is likely that additional machinery is required to form the two LD populations. We
309 currently speculate that PLIN1 transport to the LDs is gated. The involved machinery may depend
310 on the Seipin complex which probably contributes to the enrichment of PLIN1 on the surface of
311 the first LD class and restricts the movement back to the ER.

312

313 **Acknowledgements**
314 We thank Pedro Carvalho (University of Oxford) for critical reading of the manuscript and Lucas
315 Pelkmans (University of Zurich) for generous support with research infrastructure.
316 A.R.T. was supported by **ANR-MOBIL** and **ANR-21-CE11-LIPRODYN**. R.W.K acknowledges support
317 from the Swiss National Science Foundation (**SNF 31003A_159793**), the Helmut Horten
318 Foundation, and E.P. Abraham Cephalosporin fund. This publication arises from research funded
319 by the John Fell Oxford University Press Research Fund and a grant from Diabetes UK
320 (**22/0006453)**. R.W.K. acknowledges support from the imaging facility at the Dunn School of
321 Pathology, University of Oxford.

322

323

324 **Author contribution:**
325 **Conceptualization,** R.W.K; **Methodology,** M.M., R.W.K., A.R.T; **Formal analysis,** M.M., O.S., D.A.,
326 K.B., M.O, A.R.T, R.W.K.; **Investigation,** M.M., O.S., D.A., K.B., M.O, A.R.T, R.W.K.; **Resources,**
327 A.R.T. and R.W.K; **Writing – Original draft ,** R.W.K.; **Writing – Review & Editing,** M.M., O.S., A.R.T.,
328 R.W.K., **Visualization;** M.M., O.S., A.R.T., R.W.K.; **Supervision,** A.R.T. and R.W.K.; **Funding**
329 **Acquisition;** A.R.T and R.W.K.

330

331 **Declaration of Interests**
332 The authors declare no competing interests.

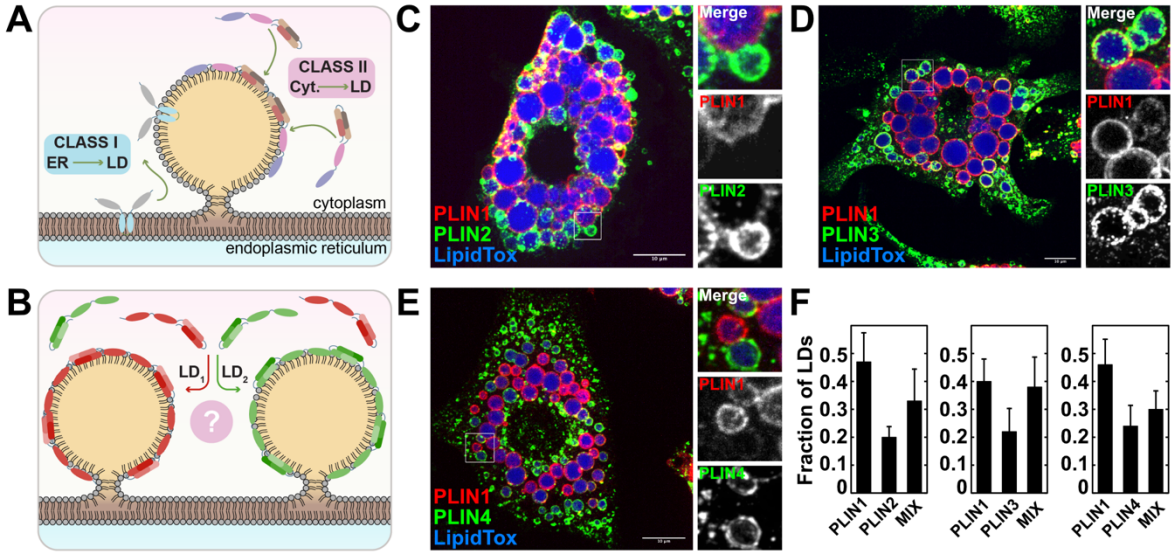
A
CLASS II
Cyt. → LD
CLASS I
ER → LD
cytoplasm
endoplasmic reticulum
B
LD1
LD2
?
C
Merge
PLIN1
PLIN2
LipidTox
D
Merge
PLIN1
PLIN3
LipidTox
E
Merge
PLIN1
PLIN4
LipidTox
F
Fraction of LDs
0.5
0.4
0.3
0.2
0.1
0
PLIN1
PLIN2
MIX
PLIN1
PLIN3
MIX
PLIN1
PLIN4
MIX

Figure 1

333

334 **Figure 1**
335 **Fatty acid feeding leads to the formation of at least two distinct LD-classes in adipocytes.**
336 **(A)** Class-I LD proteins move from the ER to the LD surface. Class-II LD proteins bind to LDs
337 directly from the cytoplasm.
338 **(B)** Segregation of class-II proteins to different LD-classes.
339 **(C)** Day 6 3T3-L1 adipocytes fed with 750µM Na^{2+}oleate for 3h. Endogenously expressed PLIN1
340 and PLIN2 were visualized by immunofluorescence. Scale bar, 10 µm.
341 **(D)** As in (C) but PLIN1 and PLIN3 were imaged.
342 **(E)** As in (C) but PLIN1 and PLIN4 were imaged.
343 **(F)** Quantification of the results in (C)-(E). n=9; n=9; n=8, for cells co-stained with PLIN1 and 2 or
344 PLIN1 and 3 or PLIN1 and 4, respectively. LD counts per replicate >100; values are expressed as
345 mean LD in each class ± SEM.
346

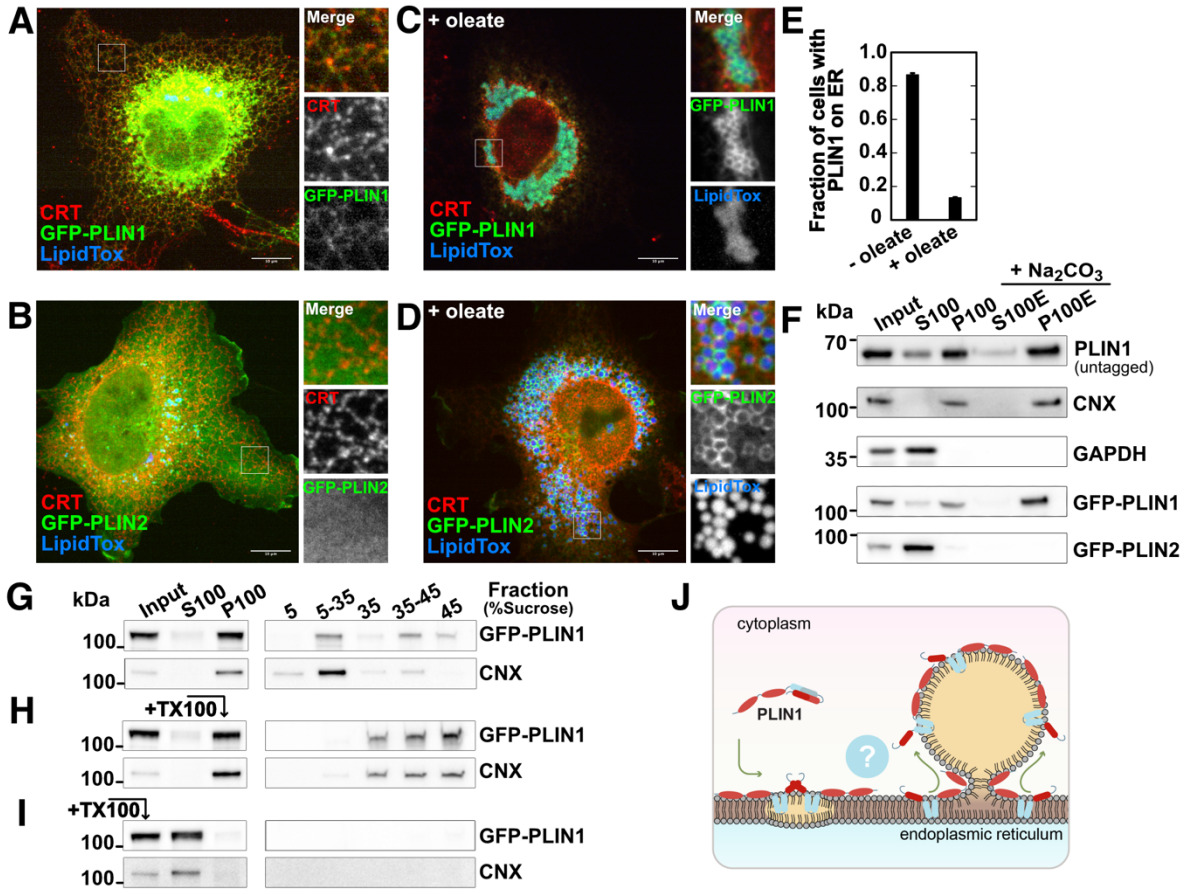
A
Merge
CRT
GFP-PLIN1
CRT
GFP-PLIN1
LipidTox
C
+ oleate
Merge
GFP-PLIN1
LipidTox
CRT
GFP-PLIN1
LipidTox
E
Fraction of cells with PLIN1 on ER
1.0
0.8
0.6
0.4
0.2
0
- oleate
+ oleate
B
Merge
CRT
GFP-PLIN2
CRT
GFP-PLIN2
LipidTox
D
+ oleate
Merge
GFP-PLIN2
LipidTox
CRT
GFP-PLIN2
LipidTox
F
+ Na2CO3
kDa
Input
S100
P100
S100E
P100E
70
PLIN1
(untagged)
100
CNX
35
GAPDH
100
GFP-PLIN1
100
GFP-PLIN2
G
kDa
Input
S100
P100
5
5-35
35
35-45
45
Fraction
(%Sucrose)
100
GFP-PLIN1
100
CNX
H
+TX100
100
GFP-PLIN1
100
CNX
I
+TX100
100
GFP-PLIN1
100
CNX
J
cytoplasm
PLIN1
?
endoplasmic reticulum

Figure 2

347

348 **Figure 2**
349 **PLIN1 is an integral membrane protein which localizes to the ER and LDs.**
350 **(A)** GFP-murinePLIN1 was expressed in COS7 cells. The ER is visualized with an antibody against
351 calreticulin (CRT). LDs are stained with LipidToxRed. Scale bar, 10 µm.
352 **(B)** As in (A) but the cells expressed GFP-PLIN2.
353 **(C)** As in (A) but with 250 µM Na^+oleate for 6h.
354 **(D)** As in (C) but the cells expressed GFP-PLIN2.
355 **(E)** Quantification of results in (A) and (C) with GFP-PLIN1 on the ER. n = 3 independent
356 experiments with >1500 cell per replicate; fraction of PLIN1 on the ER ±SD.
357 **(F)** COS7 expressing untagged PLIN1, GFP-PLIN1 or GFP-PLIN2, were fractionated followed by
358 alkaline extraction. **Input,** cell lysate; **S100, P100,** supernatant and pellet of a 100k x g
359 centrifugation, **S100E, P100E,** E denotes alkaline (Na_2CO_3) extraction. **GAPDH,** glycerolaldehyde-
360 3-phosphate dehydrogenase; **CNX,** calnexin.
361 **(G)** As in (F), but P100 was floated on a sucrose-step gradient.
362 **(H)** As in (G), but P100 was incubated with Triton X-100 before flotation.
363 **(I)** As in (H), but the cell lysate was treated with Triton X-100 before centrifugation.
364 **(J)** PLIN1 is an integral membrane protein with a membrane anchor (blue) allowing ER and LD-
365 targeting.
366

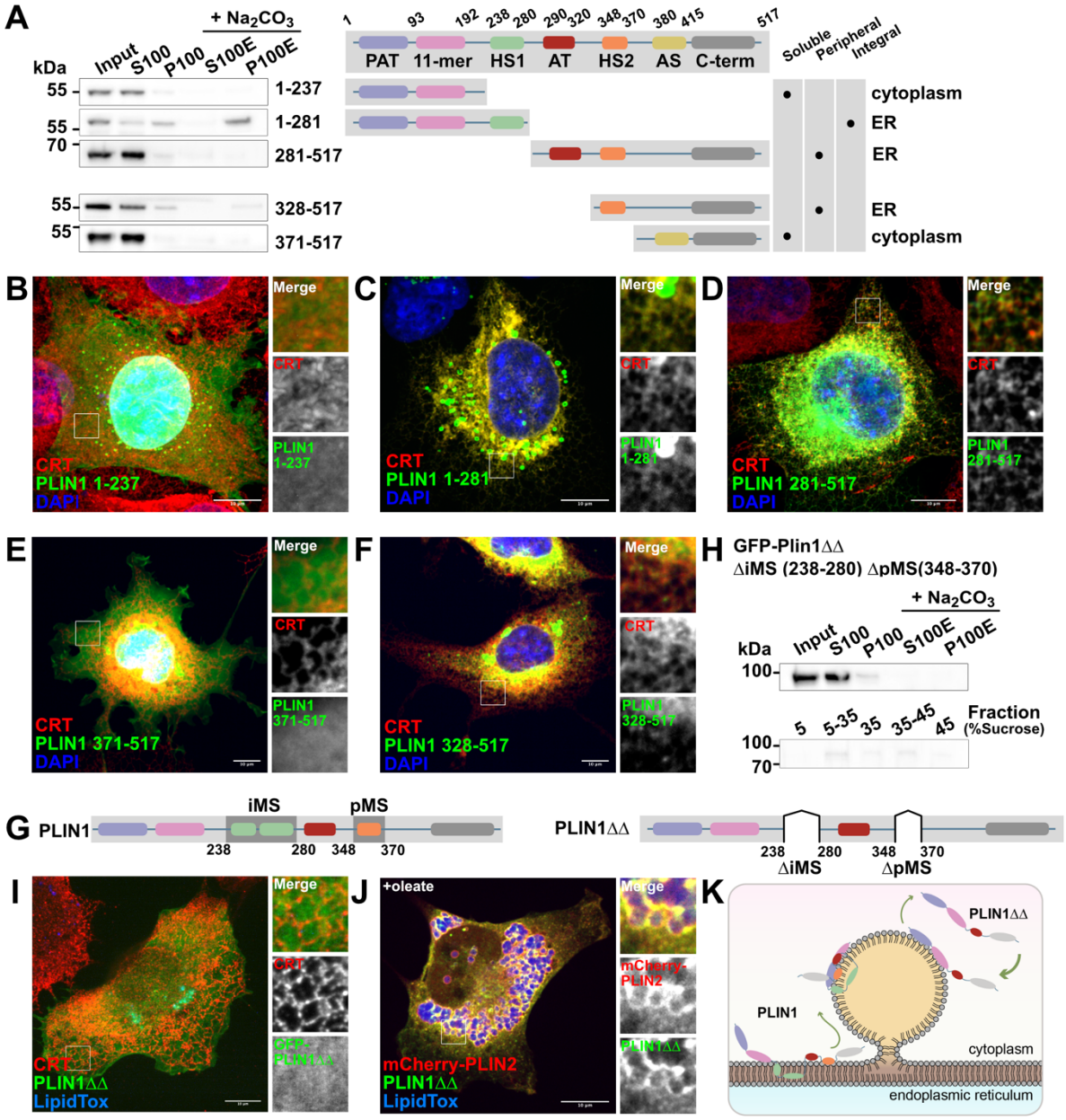
A
+ Na2CO3
kDa
Input
S100
P100
S100E
P100E
55
55
70
55
55
1-237
1-281
281-517
328-517
371-517
1
93
192
238
280
290
320
348
370
380
415
517
PAT
11-mer
HS1
AT
HS2
AS
C-term
Soluble
Peripheral
Integral
cytoplasm
ER
ER
ER
cytoplasm
B
Merge
CRT
PLIN1 1-237
DAPI
C
CRT
PLIN1 1-281
DAPI
D
CRT
PLIN1 281-517
DAPI
E
CRT
PLIN1 371-517
DAPI
F
CRT
PLIN1 328-517
DAPI
H
GFP-Plin1ΔΔ
ΔiMS (238-280) ΔpMS(348-370)
+ Na2CO3
kDa
Input
S100
P100
S100E
P100E
100
5
5-35
35
35-45
45
Fraction
(%Sucrose)
100
70
G
PLIN1
iMS
pMS
238
280
348
370
PLIN1ΔΔ
238
280
348
370
ΔiMS
ΔpMS
I
CRT
PLIN1ΔΔ
LipidTox
J
+oleate
mCherry-PLIN2
PLIN1ΔΔ
LipidTox
K
PLIN1ΔΔ
PLIN1
cytoplasm
endoplasmic reticulum

Figure 3

367

368 **Figure 3**
369 **Identification of two ER-targeting segments in PLIN1.**
370 **(A)** PLIN1 analysis by fractionation and alkaline extraction and Western-blotting with anti GFP-
371 antibody. See Fig.S3 for domain description.
372 **(B)** COS7 cells expressing a GFP-PLIN1 (1-237). The ER was visualized with an antibody to
373 calreticulin (CRT). The nuclei were stained with DAPI. Scale bar, 10 µm.
374 **(C)** As in (B) but with PLIN1 1-281.
375 **(D)** As in (B) but with PLIN1 281-519.
376 **(E)** As in (D) but with PLIN1 371-517.
377 **(F)** As in (D) but with PLIN1 328-517.
378 **(G)** Illustration of the integral membrane segment (iMS, 238-280) and the peripheral membrane
379 segment (pMS, 348-370) and PLIN1ΔΔ lacking both.
380 **(H)** As in (A) but deletion of iMS and pMS (GFP-PLIN1ΔΔ). P100 was subjected to alkaline
381 extraction (+Na_2CO_3) and floated as in Fig. 1G.
382 **(I)** As in (B) but with PLIN1ΔΔ. LDs were stained with LipidToxDeepRed.
383 **(J)** COS7 cells co-expressing m-cherry2-PLIN2, and GFP-PLIN1ΔΔ were treated with 250 µM
384 Na^+oleate for 6h.
385 **(K)** Deletion of the iMS and pMS switches PLIN1 from an integral to class-II LD protein. Domain
386 colors as in (A).
387

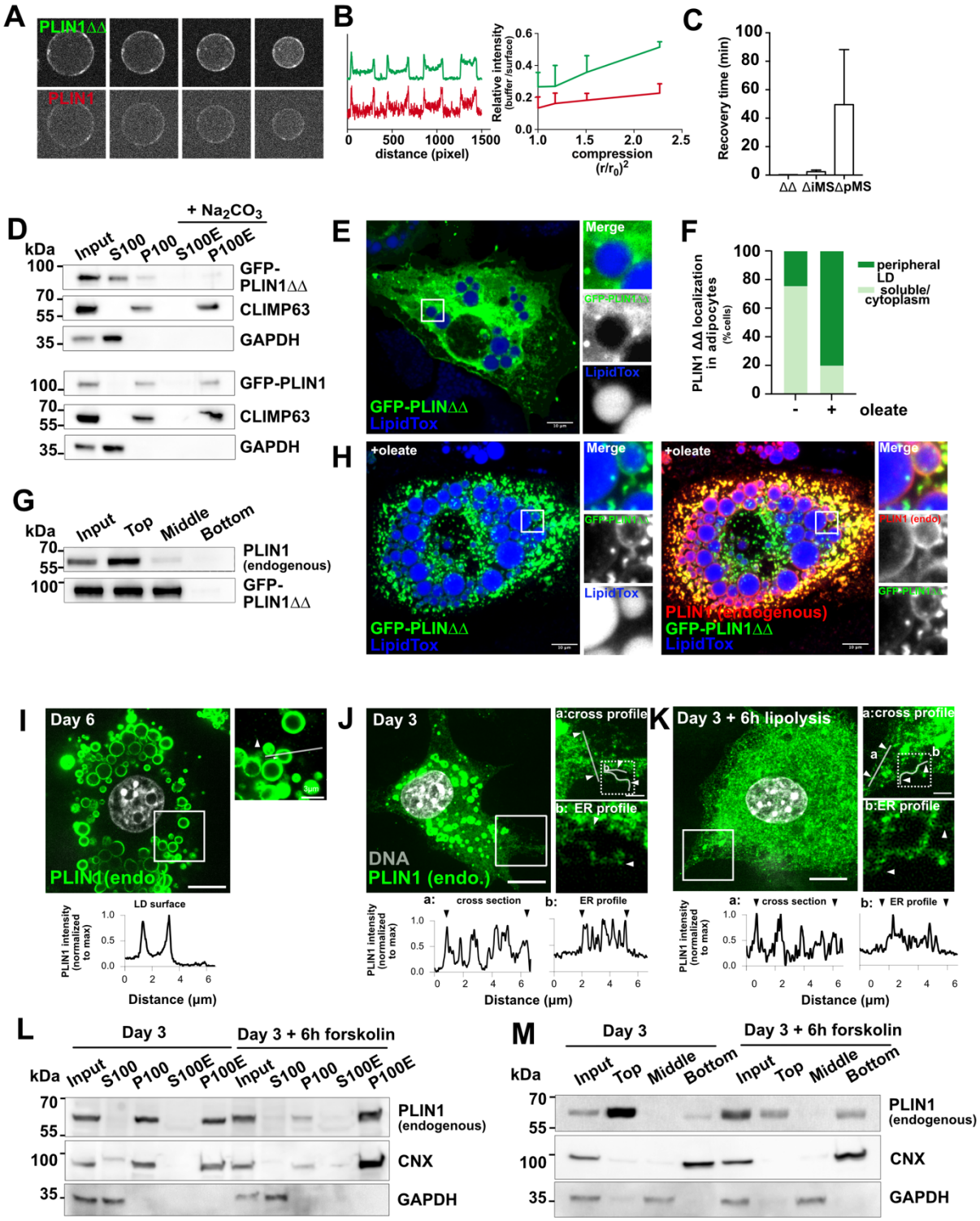
A
PLIN1ΔΔ
PLIN1
B
distance (pixel)
Relative intensity (buffer /surface)
compression (r/r0)2
C
Recovery time (min)
ΔΔ
ΔiMS
ΔpMS
D
+ Na2CO3
kDa
Input
S100
P100
S100E
P100E
GFP-PLIN1ΔΔ
CLIMP63
GAPDH
GFP-PLIN1
E
Merge
GFP-PLIN1ΔΔ
LipidTox
F
PLIN1 ΔΔ localization in adipocytes (% cells)
peripheral LD
soluble/ cytoplasm
oleate
G
Input
Top
Middle
Bottom
PLIN1 (endogenous)
H
+oleate
PLIN1 (endogenous)
I
Day 6
PLIN1(endo)
LD surface
PLIN1 intensity (normalized to max)
Distance (µm)
J
Day 3
a:cross profile
b: ER profile
DNA
PLIN1 (endo.)
cross section
ER profile
K
Day 3 + 6h lipolysis
L
Day 3
Day 3 + 6h forskolin
CNX
M

Figure 4

388

389 **Figure 4**
390 **Membrane insertion determines LD-class specificity by tuning LD binding kinetics**
391 **(A)** Localization of GFP-PLIN1ΔΔ and mCherry-PLIN1 in an buffer-in oil system with shrinking
392 aqueous phase progressively shrinks.
393 **(B)** Intensity ration of signal at the oil-buffer interface and within buffer for indicated
394 compression ratios; GFP-PLIN1ΔΔ (green), mCherry-PLIN1 (red). N=3 independent experiments;
395 mean ± SD.
396 **(C)** FRAP with oleate treated Huh7 cells expressing GFP-PLIN1ΔΔ, ΔiMS or ΔpMS. Scale bar, 10
397 µm. N = 3 experiments; results are expressed as mean ± SD.
398 **(D)** GFP-PLIN1ΔΔ or GFP-PLIN1 were expressed in 3T3-L1 cells from inducible transgenes and
399 subjected to fractionation and alkaline extraction. Labeling as in Fig. 2; **CLIMP-63,** integral ER-
400 membrane protein.
401 **(E)** As in (D) but with adipocytes. PLIN1ΔΔ was induced 6 days post differentiation with 500 ng/ml
402 anhydrotetracycline for 6h. LDs stained with LipidToxDeepRed. Scale bar, 10 µm.
403 (**F**) Percentage of cells in (E) and (H) with GFP-PLIN1ΔΔ on peripheral LDs or in the cytoplasm, N
404 = 100 cells.
405 **(G)** As in (E) but with flotation. Endogenous PLIN1 and GFP-PLIN1ΔΔ were both detected with an
406 anti PLIN1-antibody.
407 **(H)** As in (E) but with oleate for 6h. GFP-PLIN1ΔΔ is now found on peripheral LDs. PLIN1ΔΔ
408 remains excluded from the LDs covered by endogenous PLIN1. On the right, anti PLIN1-antibody
409 stains both endogenous PLIN1 on large LDs (red) and PLIN1ΔΔ on the peripheral LDs
410 (GFP+red=yellow).
411 (**I**) Endogenous PLIN1 (green) in day6 adipocytes; line plot of PLIN1 intensity (normalized to
412 maximum), as drawn in the inset. Scale bar: 10 µm, for inset 4 µm.
413 **(J)** As in (I), but at day 3. Arrowheads mark terminal points of ER.
414 **(K)** As in (J), but after addition of 10 µM forskolin for 6h (lipolysis).
415 **(L)** Fractionation and alkaline extraction of adipocytes as in (J) and (K); labels as in (D); **CNX**,
416 calnexin (integral ER-membrane protein).
417 **(M)** Flotation experiment of the cells as in (J) and (K), done as in (G).

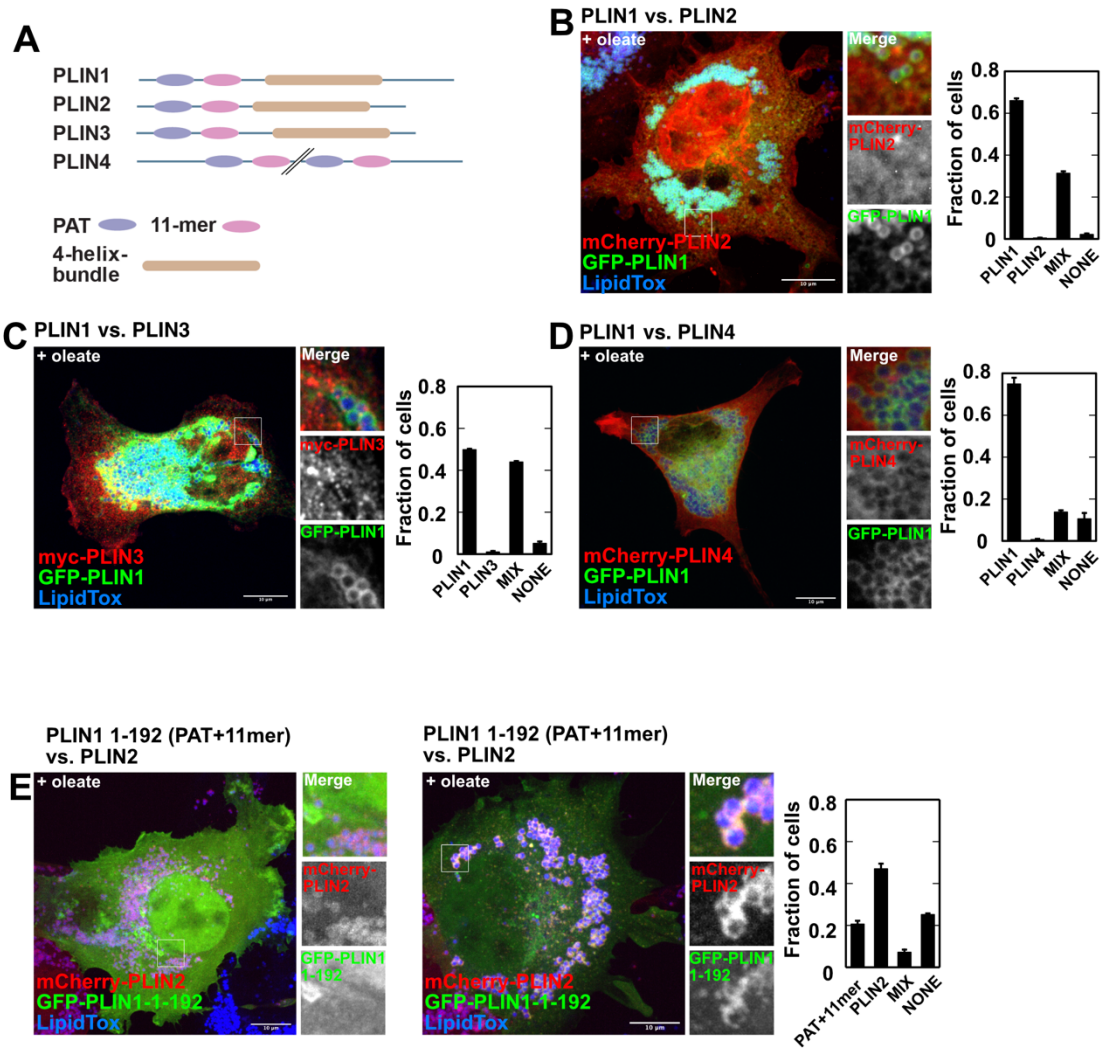

Figure S1

418

419 **Figure S1, related to Figure 1**
420 **PLIN1 excludes PLIN2, 3 and 4 from LD binding in COS7 cells.**
421 **(A)** Schematic representation of perilipin (PLIN) 1-4. The N terminal PAT (perilipin,
422 adipophilin/ADRP domain) and 11-mer regions are important for LD targeting. PLIN1-3 contain a
423 predicted four helix bundle. The PLINs were grouped into a protein family based on the sequence
424 similarity found in the PAT and 11-mer domains as well as their localization to the LD surface.
425 PLIN4 does not contain a four-helix bundle and is much larger than the other family members.
426 **(B)** COS7 cells co-expressing PLIN1 tagged at its N-terminus with GFP (GFP-PLIN1) and PLIN2
427 carrying an N-terminal mCherry2 tag (mCherry-PLIN2). 250 µM Na^+oleate was added to the
428 growth medium 6h prior to fixation. Lipid droplets were stained with LipidToxDeepRed (LipidTox).
429 The cells were automatically segmented and assigned by a support vector machine based
430 classifier into 4 groups, in which PLIN1 was exclusively found on the LD surface and PLIN2 was
431 cytoplasmic **(PLIN1)**, cells that showed only PLIN2 LD staining **(PLIN2)**, cells in which various levels
432 of PLIN2 was found on LDs together with PLIN1 **(MIX)**, and cells in which neither of the two
433 proteins was found on the LD **(NONE)**. Intensity and texture of PLIN1 and PLIN2 channels as well
434 as correlation with LipidTOXDeepRed were used as training features. n = 3 independent
435 experiments ; the results are expressed as mean ±SD. Scale bar, 10µm.
436 **(C)** As in (B) but PLIN3 tagged at its N-terminus with c-myc (myc-PLIN3) was co-expressed with
437 GFP-PLIN1. n = 3 independent experiments ; the results are expressed as mean ±SD.
438 **(D)** As in (C) but PLIN4 tagged at its N-terminus with mCherry2 (mCherry-PLIN4) was co-expressed
439 with GFP-PLIN1. n = 3 independent experiments ; the results are expressed as mean ±SD.
440 **(E)** COS7 cells co-expressing PLIN1 truncated after the 11-mer at residue 192 tagged at its N-
441 terminus with a GFP (GFP-PLIN1-1-192) and PLIN2 tagged at its N-terminus with mCherry2
442 (mCherry-PLIN2).
443

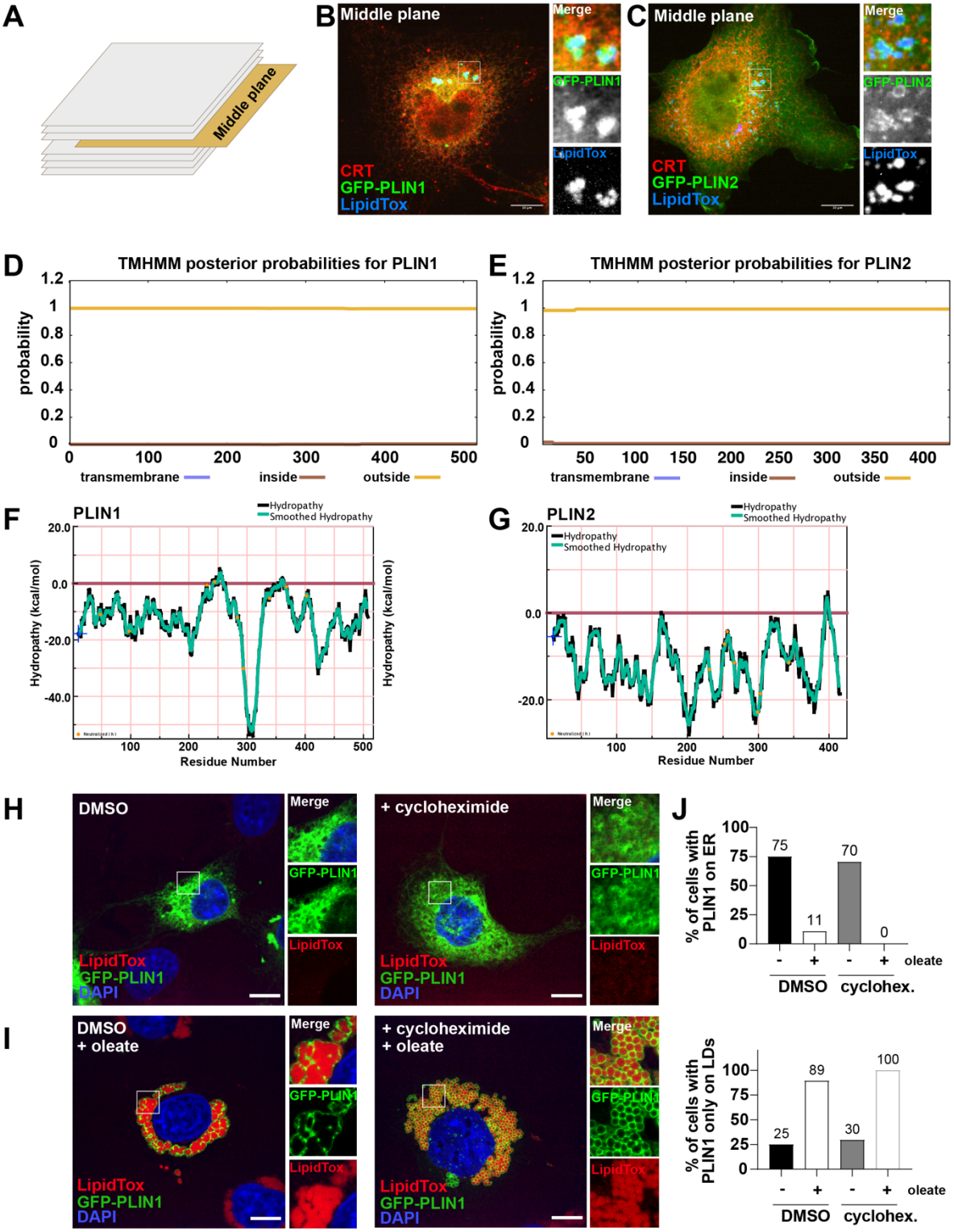

Figure S2

444

445 **Figure S2, related to Figure 2**
446 **Subcellular targeting of PLIN1 and PLIN2;**
447 **TMHMM predictions and hydropathy plot analysis for PLIN1 and PLIN2;**
448 **PLIN1 LD targeting does not require translation.**
449 **(A)** Schematic illustration of image stack and the middle plane shown in (B) and (C).
450 **(B)** COS7 cells expressing PLIN1 tagged at its N-terminus with GFP. Lipid droplets were stained
451 with LipidToxRed and the ER was visualized with an antibody specific to the endogenously
452 expressed luminal ER protein calreticulin (CRT).
453 **(C)** As in (B) but cells expressed PLIN2 with an N-terminal GFP tag (GFP-PLIN2).
454 **(D)** Topology analysis of PLIN1 using TMHMM 2.0 (Trans Membrane prediction Hidden Markov
455 Model[62] https://services.healthtech.dtu.dk/service.php?TMHMM-2.0).
456 No integral membrane domains are predicted. **Outside,** segment in cytoplasm; **Inside,** segment
457 inside the ER lumen; **transmembrane,** integral membrane segment .
458 **(E)** As in (D) but for PLIN2.
459 **(F)** Hydropathy plot analysis for PLIN1 with membrane protein explorer (MPEX)[63].
460 **(G)** As in (F) but for PLIN2.
461 **(H)** COS7 cells expressing PLIN1 tagged at its N-terminus with GFP (GFP-PLIN1). Lipid droplets
462 were stained with LipidToxRed (LipidTox) and nuclei were visualized with DAPI. Cells were
463 either treated with DMSO as a control or with 100µg/ml cycloheximide 7h prior to fixation.
464 Scale bar, 10 µm.
465 **(I)** As in **(H)** but the cells were additionally treated with 200 µM Na^+oleate for 6h prior to
466 fixation (1h after addition of DMSO or 100µg/ml cycloheximide). The results are expressed as %
467 of cells with GFP-PLIN1 on LDs.
468 **(J)** Quantification of (H) and (I). The results are expressed as % of cells with GFP-PLIN1 on ER;
469 DMSO: N=20 (-OA), N=28 (+OA); cycloheximide: N=27 (+OA), N=20 (-OA).
470
471
472
473

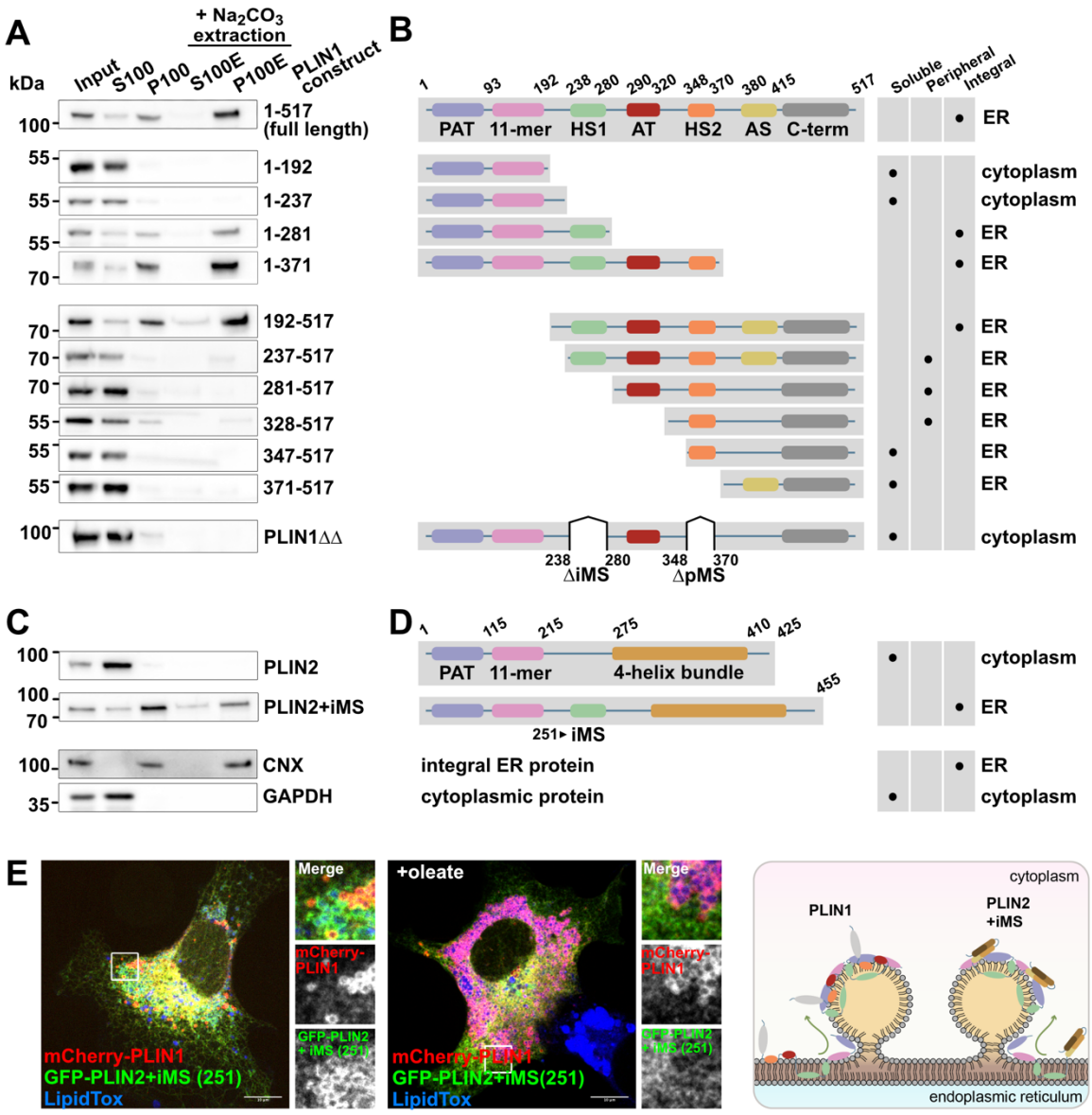

Figure S3

474

475 **Figure S3, related to Figure 3**
476 **Summary of all constructs used in the structure function analysis of PLIN1.**
477 **(A)** Structure-function analysis of PLIN1 by fractionation and alkaline extraction using the
478 indicated truncation constructs.
479 **Input,** cell lysate; **S100, P100,** supernatant and pellet of a 100k x g centrifugation step, **S100E,**
480 **P100E,** supernatant and pellet of 100k x g centrifugation after alkaline extraction with Na_2CO_3.
481 Note that PLIN1 1-517 (full length) is also shown in Fig. 2F (GFP-PLIN1) and the constructs 1-
482 237, 1-281 as well as 281-517, 328-517, and 371-517 are shown in main Fig. 3A. PLIN1ΔΔ is also
483 shown in Fig. 3H.
484 **(B)** Schematic illustration of the domains in PLIN1 and the tested truncation constructs. The
485 table summarizes the results in (A) classifying the construct as soluble when found in S100 and
486 in the cytoplasm by microscopy, as peripheral when found in S100, but seen on the ER by
487 microscopy, and integral when present in the alkaline resistant membrane pellet P100E. ER,
488 and cytoplasm is the localization as determined by microscopy. **PAT,** perilipin, adipohilin/ADRP,
489 TIP-47 domain (purple); **11-mer,** LD targeting region (pink); **HS1, 2** hydrophobic segment 1 and
490 2 (green, orange, resp.); **AT,** acidic tract (red); **AS,** amphipathic segment (yellow); **C-term,**
491 carboxy terminus with regulatory elements (grey). Classification of the constructs as soluble,
492 cytoplasmic, peripheral or integral ER membrane proteins.
493 **(C)** Fractionation and alkaline extraction experiments with GFP-PLIN2 (also shown in Fig 2F, for
494 simplicity marked as PLIN2) and GFP-PLIN2 containing the iMS core from PLIN1 inserted after
495 amino acid at position 251. For comparison with fractions in Fig. 2F the cytoplasmic marker
496 **GAPDH,** glycerolaldehyde-3-P-dehydrogenase (from Fig. 2F) and the ER membrane protein
497 marker **CNX,** calnexin (from Fig. 2F) are shown.
498 **(D)** As in (B) but PLIN2 is shown. Classification and definitions as in (B).
499 **(E)** COS7 cells were transfected with PLIN1 tagged at its N-terminus with mCherry2 (mCherry-
500 PLIN1) and PLIN2 containing the iMS core from PLIN1 inserted after amino acid at position 251
501 (GFP-PLIN1+iMS (251). The cells were additionally treated with 250 µM Na^+oleate 6h prior to
502 fixation when indicated. The illustration shows that PLIN1 and PLIN2+iMs segregate
503 preferentially to distinct LD classes showing that the iMS is critical in class specific LD nucleation
504 at the ER. Domain colours are as indicated in (B) and (D).
505

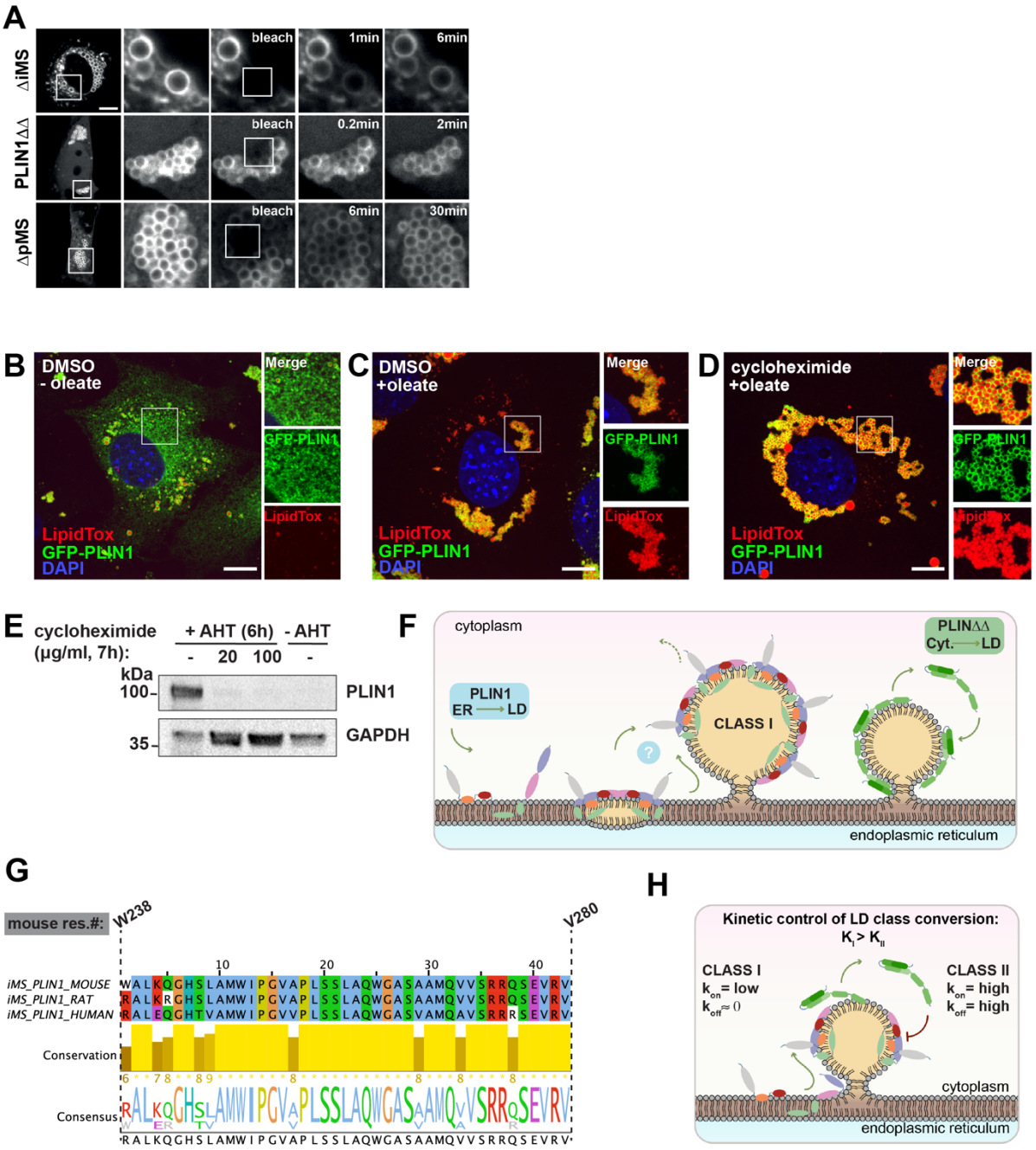

Figure S4

506

507
508 **Figure S4, related to Figure 4**
509 **Recruitment of PLIN1 from the ER to the LD surface is independent of translation**
510 **(A)** Huh7 cells expressing the indicated GFP-tagged PLIN1 constructs were subjected to
511 photobleaching and the recovery of the GFP signal within the boxed area was plotted over
512 time. **Related to Fig. 4C.**
513 **(B)** 3T3-L1 cells expressing PLIN1 tagged at its N-terminus with GFP (GFP-PLIN1) from a stably
514 integrated inducible trans-gene. Expression was induced with 500 ng/ml anhydrotetracycline
515 (AHT) over-night (total 20h). Lipid droplets were stained with LipidToxRed (LipidTox) and nuclei
516 were visualized with DAPI. Scale bar, 10 µm.
517 **(C)** As in (B) but the cells were additionally treated with Na^+oleate 3h prior to fixation.
518 **(D)** As in (C) but translation was shut off by treating the cells with 100 µg/ml cycloheximide 1h
519 before the addition of Na^+oleate.
520 **(E)** Validation of GFP-PLIN1 expression and translation shut off by cycloheximide. To induce
521 expression of GFP-PLIN1, the cells were treated with 500ng/ml anhydrotetracycline (AHT) 6h
522 prior to cell harvest. Translation was inhibited with the indicated concentrations of
523 cycloheximide 1h before treatment with AHT. As a negative control AHT was omitted (-AHT).
524 **(F)** PLIN1 is targeted to the ER membrane (brown) by the iMS (green) and the pMS (orange).
525 PLIN1 likely moves to the LD using bridge-connections or by an unknown cytoplasmic
526 intermediate that carries lipids to the LD (indicated by "?"). PLIN1ΔΔ binds to the LD directly
527 from the cytoplasm as expected for a prototypical class-II protein.
528 **(G)** Alignment of mouse, rat and human PLIN1 iMS. The regions correspond to mouse PLIN1
529 residues 238-280. The sequences were retrieved from Uniprot Q8CGN5, P43884, O60240
530 respectively, aligned using ClustalOmega https://www.ebi.ac.uk/Tools/msa/clustalo/ and
531 analysed in JalView https://www.jalview.org/ using the T-coffee algorithm for determination of
532 the consensus sequence shown below the sequence conservation bar graph.
533 **(H)** LD-binding rates of class-II proteins are faster than for class-I proteins. The steady state
534 PLIN1 ER-pool is low, slowing down the LD on-reaction. When bound to the LD, class-II proteins
535 exchange faster than class-I proteins. The resulting high affinity to LDs leads to the gradual
536 replacement of class-II by class-I proteins from the newly formed LDs.
537
538

539

540 # Experimental procedures

541 # STAR Methods

542 ## Lead contact and materials availability

543 Further information and requests for resources and reagents should be directed to and will be
544 fulfilled by the Lead Contact, Robin Klemm (Robin.Klemm@dpag.ox.ac.uk).
545

546 ## Data and code availability

547 Original/source data for in the paper is available upon request from the lead contact and in
548 Supplementary Data.
549

550 ## Method Details

551 ### Cell lines

552 COS-7 cells were a kind gift from Tom A. Rapoport (Harvard Medical School, Boston, USA). COS7
553 is a male African green monkey kidney fibroblast cell line. HEK293T cells were obtained from
554 Dharmacon (#TLP5918). HEK293T is a female human embryonic kidney cell line. 3T3-L1 pre-
555 adipocytes were from ATCC (CL-173). 3T3-L1 is a continuous sub-strain of male murine 3T3
556 (Swiss albino) cells, developed through clonal isolation.

557 ### Cell culture

558 COS-7 cells were maintained in Dulbeccos's Modified Eagle Medium with 4.5 g/l glucose and L-
559 glutamine (DMEM, Thermo Fischer Scientific, #41965062), supplemented with 10% fetal bovine
560 serum (FBS; Sigma-Aldrich, #F7524). HEK293T cells were maintained in DMEM containing 10%
561 FBS, 25 mM HEPES (Sigma-Aldrich, H4034), 1 mM sodium pyruvate (Thermo-Fisher), 2 mM
562 glutamine (Sigma-Aldrich) and 100 µM non-essential amino acids (Thermo-Fisher). All cells were
563 kept as sub-confluent cultures and were sub-cultured regularly. All cell lines were periodically
564 tested for mycoplasma and grown according to ATCC guidelines. Cells were incubated at 37°C
565 and 5% CO_2.

566 ### Pre-adipocyte maintenance

567 3T3-L1 pre-adipocytes were obtained from ATCC (CL-173) and cultured in DMEM with 4.5 g/l
568 glucose and L-glutamine (Thermo Fischer Scientific, #41965062), containing 10% calf serum (CS;
569 Sigma-Aldrich, #12133C). Cells were grown as sub-confluent cultures in 10 cm tissue culture
570 dishes (TPP) and sub-cultured regularly.

571 ### Adipocyte differentiation procedure

572 For the differentiation of 3T3-L1 pre-adipocytes into white adipocytes, the cells were first
573 grown to confluence and kept as a confluent culture for 48 hours. For differentiation in 96-well
574 format, cells were seeded at a density of 10,000 cells per well of a 96-well plate (Greiner).
575 Typically, the cells reached confluence the next day. After 48 hours of confluence
576 differentiation was induced by the addition of adipocyte differentiation medium consisting of
577 DMEM supplemented with 10% FBS, 172 nM bovine insulin (Sigma-Aldrich, #I0516), 500 µM 3-

578 Isobutyl-1-methylxanthine (IBMX, Sigma-Aldrich #I5879), and 1 µM dexamethasone
579 (Gbiosciences, #API-04). Cells were kept in differentiation medium for 48 hours. The
580 differentiation medium was then replaced by DMEM containing 10% FBS and 172 nM bovine
581 insulin. Cells were kept in the insulin medium for another 48 hours. At day four after induction
582 of differentiation the insulin medium was replaced by DMEM containing 10% FBS. The medium
583 was then refreshed every two days. Typically, cells were used for experiments at day 6 or day 8
584 after start of differentiation.
585

586 ## Method details

587 ### Transfection and subcellular fractionation and alkaline extraction

588 1.1×10^6 COS-7 cells were seeded on a 10 cm dish the one day before transfection. The next
589 morning cells were transfected with 10 µg of the plasmid of interest using GeneJuice
590 transfection reagent (Merck, #70967-3) according to the manufacturer's instructions. After 6
591 hours of incubation at 37°C the medium was replaced with fresh DMEM containing 10% FBS.
592 The cells were then incubated at 37°C/5% CO_2 overnight. The next morning the cells were
593 washed once with ice-cold PBS and then harvested in 1 mL PBS with a cell scraper. The cells
594 were briefly pelleted at 2000 g for 5 min at 4˚C, and the supernatant was discarded. The cells
595 were resuspended in 1 mL PBS containing protease inhibitor cocktail (cOmplete™, Mini, EDTA-
596 free Protease Inhibitor Cocktail; Merck, #11836153001) (PBSI) and lysed by 20 passages
597 through a bead-homogenizer (Isobiotec, 16 µm bead). A small aliquot for subsequent analysis
598 by SDS-PAGE was taken ("Input") and the remaining lysate was clarified by centrifuging for 10
599 minutes at 4°C and 2000 g. The supernatant was transferred to a 1.5 mL ultracentrifuge tube
600 (Beckman-Coulter, #357448) and the membranes were pelleted at 100,000 g for one hour at
601 4°C in a TLA 100.3 rotor (Beckman-Coulter). Afterwards the supernatant was taken off and
602 stored at -20°C ("S100") and the pellet was resuspended in 50 µL PBSI. A small aliquot of 25 µL
603 was stored at -20°C for analysis by SDS-PAGE ("P100") and the remaining 25 µL were subjected
604 to alkaline extraction by adding 75 µL of 250 mM Na_2CO_3 (pH 11) (Sigma Aldrich,
605 #A0634292404) for 15 min on ice. The sample was transferred to a 250 µL ultracentrifuge tube
606 (5 x 20 mm Beckman-Coulter, #342630) and a 50 µL of 10% sucrose cushion was placed below
607 the sample at the bottom of the tube. The samples were then centrifuged for 1 h at 100,000 g
608 and 4°C in a TLS 55 rotor (Beckman-Coulter) with the appropriate adapters (#358614). The top
609 200 µL were carefully taken off and stored at -20°C ("S100E") and the pellet was resuspended in
610 50 µL PBS and stored at -20°C ("P100E"). The samples were subsequently analyzed by SDS-PAGE
611 and western blotting to PVDF membranes (see respective sections).

612 ### Denaturing SDS polyacrylamide gel electrophoresis (PAGE) and immunoblotting

613 SDS-PAGE analysis was carried out either with 10% gels (TGX FastCast acrylamide Kit 10%; Bio-
614 Rad) or precast 4-15% gradient gels (Mini-PROTEAN TGX precast gel; Bio-Rad). The protein
615 concentration was determined using the Pierce 660 nm protein assay (Thermo-Fisher). Samples
616 were denatured by the addition of SDS sample buffer (62.5 mM Tris-HCl, pH 6.8, 10% glycerol,
617 2% SDS, 0.002% bromophenol blue, 5% β-mercaptoethanol) and boiled for 10 minutes at 95°C.
618 For western blotting the proteins were transferred to polyvinylidene difluoride (PVDF)

619 membranes using the Trans-Blot Turbo RTA Mini PVDF Transfer Kit (Bio-Rad) and the Trans-Blot
620 Turbo Transfer System (Bio-Rad). Membranes were blocked for one hour in 3% BSA/TBST (20
621 mM Tris-HCl, pH 7.4, 137 mM NaCl, 0.1% Tween 20) at room temperature. The incubation with
622 the primary antibody was carried out in 3% BSA/TBST either for 1h at room temperature or
623 overnight at 4°C. After extensive washing with TBST the membranes were incubated with the
624 secondary HRP-conjugated antibodies diluted in 5% skim milk/TBST for 1h at room
625 temperature. The membranes were again extensively washed with TBST and the ECL reagent
626 (GE Healthcare) was mixed and added for 1 min afterwards. Images were acquired using Vilber-
627 Lourmat instrument and its software.
628

629 **Lipid droplet flotation**

630 One 10 cm dish of day 6 3T3-L1 adipocytes was used. The cells were washed with ice-cold PBS
631 and subsequently harvested by scraping in PBS. The cells were centrifuged at 600 g, 4°C for 5
632 minutes. The supernatant was discarded, and the pellet containing the cells was resuspended in
633 1 mL PBS supplemented with protease inhibitor (cOmplete™, Mini, EDTA-free Protease
634 Inhibitor Cocktail; Merck). The cells were lysed by 20 passages through a bead homogenizer (16
635 µm bead, Isobiotec) and the lysate was clarified at 600 g, 4°C for 10 minutes. The supernatant
636 was transferred to a new 1,5 mL tube and supplemented with 60% sucrose/PBS to a final
637 concentration of 12% sucrose. 600 µL of the lysate were transferred to an ultracentrifuge tube
638 (5 x 41 mm, Beckman-Coulter, #344090) and centrifuged in an MLS-50 rotor (Beckman-Coulter)
639 at 100,000 g, 4°C for 1h. After the centrifugation the tubes were sealed, and the lower
640 boundary of the floating lipid droplet fraction was marked. The tubes were flash frozen in liquid
641 nitrogen and the top and were collected by cutting the frozen tube. The middle fraction was
642 collected after thawing and the remaining pelleted fraction was washed once with PBS and
643 then resuspended in PBS. All samples were then stored at -20°C until further analysis by SDS-
644 PAGE.

645 **Membrane flotation**

646 Flotation experiments were carried out using five 10 cm dishes COS7 cells. Cells were washed
647 with ice-cold PBS and subsequently harvested by scraping in PBS. The cells were briefly pelleted
648 at 600 g, 4°C for 5 minutes. The supernatant was discarded, and the pellet was resuspended in
649 1 mL PBS supplemented with protease inhibitor (cOmplete™, Mini, EDTA-free Protease
650 Inhibitor Cocktail; Merck). The cells were lysed by approx. 20 passages through a bead
651 homogenizer (Isobiotec, 16 µm bead) and the lysate was cleared from debris at 600 g, 4°C for
652 10 minutes. 100 µL supernatant was collected and stored at -20°C; the remaining supernatant
653 was transferred to a 1.5 mL ultracentrifuge tube (Beckman-Coulter) and centrifuged in a
654 TLA 100.3 rotor (Beckman-Coulter) at 100,000 g, 4°C for one hour. The supernatant was
655 transferred to a new 1.5 mL tube and stored at -20°C for later analysis. The pellet was
656 resuspended in 36 µL PBS supplemented with protease inhibitor and 10 µL were stored for later
657 analysis at -20°C. The remaining 26 µL were supplemented with 150 µL of 60% sucrose (w/v). To
658 remove the ribosomes from the membranes 24 µL puromycin (10 mg/mL) were added to a final
659 concentration of 2,5 M puromycin and 45% sucrose. The reaction was incubated at RT for 30
660 minutes. 300 µL of 35% sucrose (w/v) were added to a 600 µL ultracentrifuge tube (Beckman-
661 Coulter) and the resuspended pellet fraction in 45% sucrose (w/v) was loaded to the bottom of

662 the tube. Finally, 150 µL of 5% sucrose (w/v) were pipetted on top, the interphases were
663 marked, and the sample centrifuged in a MLS 50 rotor (Beckman-Coulter) at 150,000 g, 4°C for
664 3h. The tubes were subsequently frozen in liquid nitrogen and the fractions separated by
665 cutting the tube at the interface marks using a clean scalpel. The fractions that were collected
666 are the top fraction with 5% sucrose, the interphase between 5% and 35% sucrose, the 35%
667 sucrose fraction, the interphase between 35% and 45% sucrose and the bottom fraction with
668 45% sucrose. The protein concentration of the fractions was determined, and equal amounts
669 analyzed by SDS-PAGE.

670 **Indirect immunofluorescence**

671 For indirect immunofluorescence experiments cells were trypsinized and transferred either to
672 Ø 18 mm cover glasses (No. 1; VWR) in 12-well tissue culture plates (TPP) or to 96-well plates
673 (Greiner) and cultured using DMEM supplemented with 10% of the respective serum (calf
674 serum CS for 3T3-L1 or FBS for COS7 and differentiated adipocytes). Differentiated adipocytes
675 were cultured for at least two days after trypsinization to ensure proper settling of the cells.
676 Cells were fixed with 4% paraformaldehyde (PFA; Electron Microscopy Sciences) at 37°C for 30
677 minutes. After washing three times with PBS, cells were permeabilized for 15 minutes either
678 with 0.1% Triton-X100 in PBS, or, when PLIN2 or PLIN3 or 4 were stained in adipocytes, 0.2%
679 saponin and 1% CS in PBS. Cells were again washed and incubated with primary antibodies in
680 blocking solution (PBS supplemented with 1% CS) for 1 h at RT. After washing, the cells were
681 incubated with fluorescently labeled secondary antibodies in blocking solution for 1h at RT. For
682 lipid droplet visualization HCS LipidTOX™ Green/Red/Deep Red dyes (Thermo-Fisher,
683 #H34475/#H34476/3H34477, respectively) were used at 1:500 dilution in PBS. Nuclei were
684 counterstained using DAPI (Thermo-Fisher) at a concentration of 0.4 µL/mL for 10 minutes at
685 RT. Cell outline staining, if applied, was done using Atto 490LS NHS-Ester (ATTO-TEC) at a
686 dilution of 1:800,000 in carbonate buffer for five minutes at RT.
687 Cover glasses were mounted onto Superfrost Excell glass slides (Thermo-Fisher) using
688 Fluoromount G (SouthernBiotech). Image acquisition was performed as described under
689 "Microscopy".

690 **Determination of protein concentration**

691 Protein concentration was determined in 96-well plates using the Pierce™ 660nm Protein Assay
692 (Thermo-Fisher) according to the manufacturer's manual. A standard-curve was produced with
693 a BSA solution ranging from 50-2000 µg/mL.
694

695 **Microscopy**

696 Confocal fluorescent microscopy was done on a Nikon Eclipse Ti-E microscope with enhanced
697 CSU-W1 spinning disk (Microlens-enhanced dual Nipkow disk confocal scanner, wide view
698 type), a Nikon CFI PlanApo 100x oil immersion objective (NA 1.49), and a sCMOS PCO Edge 5.5
699 camera (PCO, 2560x2160 pixels).
700 For automated confocal microscopy a Yokogawa CellVoyager 7000 spinning disk confocal
701 microscope with enhanced CSU-X1 spinning disk (Microlens-enhanced dual Nipkow disk
702 confocal scanner, wide view type), a 40x air objective (NA 1,15) or 60x water immersion (NA
703 1,2), and three Neo sCMOS cameras (Andor, 2560x2160 pixels) were used. 108 sites were

704 acquired per well of a 96-well plate with seven confocal planes of 1 µm thickness per site,
705 which were maximum intensity projected before saving. The signals for UV (405 nm) and far-
706 red (640 nm) as well as green (488 nm) and Atto490LS (675 nm) signals were acquired in dual-
707 camera mode. Red signal (561 nm) was acquired separately.
708 Images for parts of Fig. 4, S4 and S2H-I were captured on an Olympus SpinSR10 spinning disc
709 confocal system fitted with an Olympus IX-83 frame, a Yokogawa CSU-W1 SoRa super-
710 resolution spinning disc module, a Photometrics Prime BSI camera and a 60× objective (1.5 NA,
711 UPLAPOHR60x), using Olympus cellSens Dimension software. When indicated the images were
712 post-processed using an OSR filter (standard) and deconvolved (constrained iterative, maximum
713 likelihood, 5 iterations) using Olympus cellSens Dimension software (version 3.1.1).
714

715 **Automated image analysis**

716 The acquired images were analyzed using CellProfiler (https://cellprofiler.org/). When
717 necessary the cell profiler pipelines were run on the high-performance cloud computing system
718 "ScienceCloud" at the University of Zurich. Analysis pipelines were composed of generic or
719 partially customized modules as described in (Battich, Stoeger, & Pelkmans, 2015). Individual
720 cells were segmented with nuclei as primary objects that were identified based on DAPI signal,
721 and cell outlines were determined from Atto490LS signal using iterative segmentation based on
722 a watershed algorithm and related to nuclei as secondary objects. After cell segmentation the
723 background of all stainings of interest was subtracted and single-cell based features like area,
724 shape, intensities and textures were extracted using the modules "MeasureObjectAreaShape",
725 "MeasureObjectIntensity", and "MeasureTexture". Subsequent analysis was done with Matlab
726 (Mathworks).

727 **Single cell classification by support vector machines (SVMs)**

728 Single cells were classified using user supervised machine learning with a custom Matlab script
729 CellClassifier (Rämö, Sacher, Snijder, Begemann, & Pelkmans, 2009). The classifier is based on
730 support vector machine algorithm (SVM). In general, the classifiers were trained to identify and
731 remove cells that were miss-segmented using nuclear area, nuclear shape, intensity, and
732 textures as training features. Cells which overlapped with the border of an individual imaging
733 site were automatically identified and removed. Furthermore, experiment specific SVMs were
734 trained using intensity, channel correlation and texture as training features.
735

736 **Cloning of truncations and deletion mutants**

737 All truncation- and deletion-mutants were cloned by restriction ligation into the mEGFP-C1
738 using *Hind*III and *Kpn*I restriction sites. The mEGFP-C1 plasmid was a kind gift from Michael
739 Davidson (Addgene plasmid #54759).
740

741 **Cloning of GFP-PLIN2-251InsIMs**

742 Cloning of the PLIN2 domain swap mutant carrying the core iMS (PLIN1 amino acids 238-268) of
743 PLIN1 was done by insertion of the iMS sequence into mEGFP-C1-PLIN2 after amino acid 251 of
744 the PLIN2 sequence. The insertion was done using the Q5 Site-Directed Mutagenesis Kit (NEB)

745 and design of respective primers using the NEBaseChanger online tool (http://
746 nebasechanger.neb.com/).
747

748 **Generation of stable cell line inducibly expressing GFP-PLIN1**

749 The stable 3T3-L1 cells with inducibe GFP-PLIN1 or GFP-PLIN1ΔΔ (Δ238-280-Δ348-370),
750 respective transgenes were generated by lentiviral gene transfer using the pINDUCER20
751 construct and Gateway™ cloning technology. The pInducer20 was a kind gift from Stephen
752 Elledge (Addgene #44012). The respective transgenes were first sub-cloned by TOPO cloning
753 into a Gateway™ entry vector (pENTR™/D-TOPO™; Thermo-Fisher) and subsequently
754 recombined into the pINDUCER20 vector using the Gateway™ LR Clonase™ II Enzyme mix
755 (Thermo-Fisher). Production of lentiviruses and transduction of cells was performed as
756 described below.
757 The cell lines were subsequently established by selecting positively transduced cells using G418
758 selection (1 mg/mL) for several passages.
759 Expression of the respective transgene was usually induced with 500 ng/mL
760 anhydrotetracycline (ATC) for the indicated time-frames.
761

762 **Preparation of sodium oleate**

763 To prepare a solution of sodium oleate, 30 mL of double-distilled water were warmed up in the
764 microwave to approx. 40°C and 400 µL of 5 M NaOH were added. While constantly stirring, 400
765 µL of oleic acid (Sigma-Aldrich) were slowly added and the solution was stirred for another five
766 minutes (stock concentration 41 mM). If micelles where still visible, additional NaOH was added
767 until all micelles disappeared. The solution was sterile filtered through a 0.22 µm sterile filter,
768 aliquoted and stored at -20°C. Using 147 µL of the solution per 25 mL of culture medium
769 resulted in a final concentration of 250 µM.
770

771 **Cell treatments**

772 Lipolysis was induced in differentiating adipocytes by addition of 1 mM forskolin in the medium
773 (or vehicle, DMSO) to the final concentration of 10µM, for 6 hours. Oleate uptake was done by
774 adding sodium oleate to the medium in the indicated concentration for 6 hours. Protein
775 synthesis was inhibited by incubating cells in the medium containing cycloheximide (or DMSO
776 control) to final concentration of 100µg/ml for the indicated time.
777

778 **Cover glasses acid wash**

779 Cover glasses (Ø 18 mm; VWR No. 1) were placed in a ceramic rack and submerged in 2 M HCl
780 for 15 minutes. The coverslips were rinsed under tap water for 30 minutes and then washed
781 three times with double-distilled water. Finally, the coverslips were rinsed in ethanol, sterilized
782 under UV-light for 30 minutes and stored in a closed container in a tissue culture hood.
783

784 **Production of lentivirus for gene transfer**

785 Lentivirus for gene transfer and integration of pINDUCER constructs was produced in HEK 293T
786 cells (Dharmacon). The cells were cultured in DMEM supplemented with 10% FBS, 25 mM

787 HEPES (Sigma-Aldrich, H4034), 1 mM sodium pyruvate (Thermo-Fisher), 2 mM glutamine
788 (Sigma-Aldrich) and 100 µM non-essential amino acids (Thermo-Fisher) on 10 cm dishes until
789 reaching approx. 70% confluency. The cells were transfected using the calcium phosphate
790 method with the three components necessary for the lentiviral packaging: 10 µg of the
791 pINDUCER expression vector containing the construct of interest, 6.5 µg psPAX2 (Addgene #
792 12260), the viral genome packaging plasmid, and 3.5 µg pMD2.G (Addgene # 12259), encoding
793 for the viral envelope components were gently mixed with H_2O to a total volume of 597 µl. This
794 was mixed with 682 µl 2x HBSS (Hank's Balanced Salt Solution), and 85 µl 2M $CaCl_2$ were added
795 followed by 30 min incubation at RT. The entire transfection mix was added dropwise to the
796 cells and incubated for approx. 12h at 37˚C, 5% CO_2. After that the medium was replaced by
797 DMEM supplemented with 5% FBS. The media containing the lentiviral particles was collected
798 at 24, 48, and 60 hours after changing the medium. The individual fractions were sterile filtered
799 through a 0.45 µm filter, pooled and stored at 4°C. The virus particles were then concentrated
800 to approx. 200 µL final volume using an Amicon Ultra-15 centrifugal filter unit (Merck) with a
801 molecular weight cut-off of 100 kDa (Amicon "Ultra – 15 centrifugal filter"; 100 kDa MW-cut
802 off). The filtrate was brought to 1 mL final volume with DMEM supplemented with 10% CS and
803 immediately used for transduction of 3T3-L1 cells as described below.
804
805 **Transduction of 3T3-L1 preadipocytes with lentivirus**

806 3T3-L1 cells were grown in 6-well plates until 50-60% confluency before the medium was
807 replaced by the concentrated virus mixture supplemented with 8 µg/mL polybrene (Sigma-
808 Aldrich, #107689). After overnight incubation the medium was replaced by DMEM
809 supplemented with 10% CS. Cells were further selected or subjected to single clone dilution as
810 described below.
811
812 **Single cell classification by support vector machines (SVMs)**

813 Single-cell data obtained after automated image analysis was further analyzed using
814 CellClassifier (Rämö, Sacher, Snijder, Begemann, & Pelkmans, 2009), a classifier software based
815 on SVMs for supervised machine learning. In general, for all datasets SVMs were trained to
816 identify and remove cells that were miss-segmented based on features like nuclear area,
817 nuclear shape, intensity, and texture features. Also, datasets were automatically cleansed of
818 cells which touch the border of an individual imaging site. Furthermore, experiment specific
819 SVMs were trained e. g. for identifying transfected cells or cells which show a specific
820 phenotype.
821
822 **In vitro experiments**

823 The purification protocol for LDs from cells expressing fluorescently tagged LD proteins was the
824 same as in Ajjaji et al. 2019. Briefly, cells from 5 x 15 cm dishes were harvested, washed once in
825 ice-cold PBS, and lysed using a 30G needle in 1ml 20 mM Tris-EDTA buffer containing complete
826 protease and phosphatase inhibitor tablets at pH 7.5. To isolate LDs, 1ml of respective cell
827 lysates were mixed with 1 ml 60% sucrose in 20 mM Tris-EDTA buffer supplemented with
828 protease inhibitors, overlaid with 20%, 10% and 0% in buffered sucrose on top of one another
829 in 5 ml Ultra-Clear centrifuge tubes (Beckman). Gradients were centrifuged for 16 h at 100,000

830 x *g* and 4 °C, using an SW60 rotor in a Beckman L8-70 centrifuge, and 300 µL were collected
831 from the top as the LD fraction.
832
833 In vitro experiments were performed in HKM buffer: 50 mM Hepes, 120 mM K^+OAc, and 1 mM
834 $MgCl_2$ (in Milli-Q water) at pH 7.4. To create buffer-in-oil drops, a buffer-diluted LD fraction was
835 mixed with an excess of triolein by vortexing, as previously done in Ajjaji et al. 2019. The
836 shrinkage of the buffer compartment was based on water evaporation of the aqueous drops,
837 with the proteins at their surface, during imaging for 10 to 15 min on PDMS-coated glass slides.
838
839
840 **Fluorescence recovery after photo-bleaching FRAP experiments**

841 For FRAP experiments, we bleach the signal on a collection of drops and monitor the signal
842 recovery. The background signal, e.g. from the cytosol, is removed from the recorded signal,
843 which was at the end normalized by intrinsic bleaching of non-bleached areas. We used
844 GraphPad Prism to fit the FRAP recovery curves with a non-linear regression and the
845 exponential « one-phase association model ». The characteristic recovery time is extracted
846 from the model.
847
848 **Transfections**

849 When indicated Huh7 cells (60-70% confluence) were exposed for 1hr to 500 µM oleic acid
850 coupled to BSA (1% v:v) to induce LD formation and then cells were transfected with 3 µg of
851 plasmid DNA/mL using Polyethylenimine HCl MAX (Polysciences, Inc) following the
852 manufacturer's instructions.
853
854 **Quantification and statistical analysis**

855 Number of samples and replicates in an experiment, as well as dispersion (standard deviation,
856 SD, standard error of the mean, SEM), are reported for each figure in the respective legends.
857 Quantification of experimental data are described in relevant Method sections.
858
859

860 ## KEY RESOURCES TABLE

REAGENT or RESOURCE	SOURCE	IDENTIFIER
Antibodies		
Mouse monoclonal c-Myc, 1:200	Santa Cruz	Cat#: sc-40
Rabbit polyclonal Calreticulin, 1:1000	Abcam	Cat#: ab2907
Mouse monoclonal FLAG, 1:200	Sigma-Aldrich	Cat#: F3165
Mouse monoclonal HA, 1:200	Roche	Cat#: 11583816001
Goat polyclonal PLIN1, 1:200	Abcam	Cat#: ab61682
Rabbit monoclonal PLIN1, 1:200 (Fig4 I-M)	Cell Signaling	Cat#: #9349
Rabbit polyclonal PLIN2, 1:200	Abcam	Cat#: ab52355
Rabbit polyclonal PLIN3, 1:200	Millipore	Cat#: ABS482
Rabbit polyclonal PLIN4, 1:200	Sigma-Aldrich	Cat#: ABS526
Rabbit polyclonal Calnexin (CNX), 1:200	Proteintech	Cat#: 10427-2-AP
Rabbit polyclonal CKAP4 (CLIMP63), 1:200	Bethyl Laboratories	Cat#: A302-257A
Donkey anti-goat IgG Alexa Fluor 488, 1:500	Thermo-Fisher	Cat#: A11055
Donkey anti-goat IgG Alexa Fluor 568, 1:500	Thermo-Fisher	Cat#: A11057
Donkey anti-goat IgG Alexa Fluor 647, 1:500	Thermo-Fisher	Cat#: A21447
Donkey anti-mouse IgG Alexa Fluor 488, 1:500	Thermo-Fisher	Cat#: A21202
Donkey anti-mouse IgG Alexa Fluor 568, 1:500	Thermo-Fisher	Cat#: A10042
Donkey anti-mouse IgG Alexa Fluor 647, 1:500	Thermo-Fisher	Cat#: A31571
Donkey anti-rabbit IgG Alexa Fluor 488, 1:500	Thermo-Fisher	Cat#: A21206
Donkey anti-rabbit IgG Alexa Fluor 568, 1:500	Thermo-Fisher	Cat#: A10042
Donkey anti-rabbit IgG Alexa Fluor 647, 1:500	Thermo-Fisher	Cat#: A31573
Donkey anti-goat HRP, 1:2500	Bethyl	Cat#: A50-201P
Donkey anti-mouse HRP, 1:5000	Promega	Cat#: W4021
Donkey anti-rabbit HRP, 1:5000	Promega	Cat#: W4011
Biological samples		
N/A		
Chemicals, peptides, and recombinant proteins		
DMEM	GIBCO	Cat#41965-039; CAS/RRID: N/A
Fetal bovine serum	Sigma-Aldrich	Cat#F7524; CAS/RRID: N/A
Calf serum	Sigma-Aldrich	Cat#12133C; CAS/RRID: N/A
OptiMEM	GIBCO	Cat#11058-021; CAS/RRID: N/A
Non-essential amino acids	Sigma	Cat#M7145; CAS/RRID: N/A
Sodium Pyruvate	GIBCO	Cat#11360 070; CAS: 113-24-6
Puromycin	Invivogen	Cat#ant-pr-1; CAS: 58-58-2
Geneticin G418	Invivogen	Cat#ant-gn-1; CAS: 108321-42-2
Paraformaldehyde	Electron Microscopy Sciences	Cat#15711; CAS: 50-00-0
Triton X-100	Thermo Fisher Scientific	Cat#28314; CAS: 9002-93-1

Hexadimethrine bromide	Sigma-Aldrich	Cat#107689; CAS: 28728-55-4
Oleic Acid	Sigma-Aldrich	Cat#O1383-5G; CAS: 112-80-1
HCS LipidTOX Red Neutral Lipid Stain	Thermo-Fisher	Cat#H34476; CAS: N/A
HCS LipidTOX Deep Red Neutral Lipid Stain	Thermo Fisher Scientific	Cat#H34477; CAS: N/A
Fluoromount-G	SouthernBiotech	Cat#0100-01; CAS: 0100-01
Dexamethasone	G-Biosciences	Cat#API-04; CAS: 50-02-2
3-Isobutyl-1-methylxanthine	Sigma-Aldrich	Cat#I5879; CAS: 28822-58-4
Insulin	Sigma-Aldrich	Cat#I0516-5ML; CAS: 11070-73-8
Cycloheximide	Sigma-Aldrich	Cat#C7698; CAS: 66-81-9
Forskolin	Sigma-Aldrich	Cat#F3917-10MG; CAS: 66575-29-9
Atto490LS NHS Ester	Atto-tec	Cat#AD 490LS-31; CAS/RRID: N/A
Alexa Fluor 647 NHS Ester	Life Technologies	Cat#SE-af647; CAS/RRID: N/A
cOmplete, Mini Protease Inhibitor Cocktail	Sigma Aldrich	Cat#11836153001; CAS/RRID: N/A
Ionic Detergent Compatibility Reagent for Pierce	Thermo Fisher Scientific	Cat#22663; CAS/RRID: N/A
D-Glucose [U-14C]	Hartmann analytic	Cat#MC 144W; CAS/RRID: N/A
Doxycycline hyclate	Sigma-Aldrich	Cat#D9891-1G; CAS: 24390-14-5
Chloroform	Rathburn Chemicals	Cat#RH1009; CAS: 67-66-3
Methanol	Biosolve Chemicals	Cat#13687802; CAS: 67-56-1
Propanol	Sigma-Aldrich	Cat#650447; CAS: 67-63-0
Critical commercial assays		
Pierce 660nm Protein Assay Reagent	Thermo Fisher Scientific	Cat#22660; CAS/RRID: N/A
GFP-Trap Magnetic Agarose	ChromoTek	Cat# gtma-10
Deposited data		
Mouse 3T3-L1 cells	ATCC	Cat#CL-173; RRID: CVCL_0123
Monkey COS-7 cells	Tom A. Rapoport, Harvard Medical School, Boston, USA	N/A; RRID: CVCL_0224
Human HEK293T cells	Dharmacon	Cat#TLP5918; RRID: CVCL_0063
Experimental models: Cell lines		
COS-7	Tom A. Rapoport (Harvard Medical School, Boston, USA)	

3T3-L1	ATCC	CL-173
HEK293T	Dharmacon	
Experimental models: Organisms/strains		
N/A		
Oligonucleotides		
Cloning primers for GFP-PLIN1 mutations	This study	Supplementary Table
Recombinant DNA		
mEGFP-N1	Michael Davidson Lab	Addgene 54767
mEGFP-C1	Michael Davidson Lab	Addgene 54759
mCherry2-C1	Michael Davidson Lab	Addgene 54563
mCherry2-N1	Michael Davidson Lab	Addgene 54517
pINDUCER20	Stephen Elledge Lab	Addgene 44012
pINDUCER21	Stephen Elledge & Thomas Westbrook Lab	Addgene 46948
APEX2-GBP	Rob Parton Lab	Addgene 67651
psPAX2	Didier Trono Lab	Addgene 12260
pMD2.G	Didier Trono Lab	Addgene 12259
GFP-PLIN1	This study	N/A
GFP-PLIN2	This study	N/A
GFP-PLIN3	This study	N/A
GFP-PLIN1 1-92, 1-237, 1-281, 1-371	This study	N/A
GFP-PLIN1 192-517, 237-517, 281-517, 328-517, 347-517, 371-517	This study	N/A
GFP-PLIN1-ΔΔ (Δ238-280 Δ348-370)	This study	N/A
GFP-PLIN2+251InsiMS	This study	N/A
cDNA Mouse PLIN1	Dharmacon	MMM1013-202799812
cDNA Mouse PLIN3	Dharmacon	MMM1013-202764453
Software and algorithms		
MATLAB		https://www.mathworks.com/products/matlab.html
CellProfiler	Carpenter et al., 2006	https://github.com/pelkmanslab/CellProfilerPelkmans
CellProfiler Pelkmans Lab	Battich et al., 2015	https://github.com/pelkmanslab/CellProfilerPelkmans/tree/master/Modules
ImageJ	National Institutes of Health, USA	https://imagej.net/Welcome RRID: SCR_003070
Other		
Round microscope cover glasses, 18 mm, No. 1	VWR	Cat#631-1580; CAS/RRID: N/A
Nikon Eclipse Ti E with CSU-W1 spinning disk	Nikon	
Yokogawa CellVoyager 7000 with CSU-X1 spinning disk	Yokugawa	
Leica SP5 confocal laser scanning microscope	Leica	

861 **References**

862 1. Rosen, E.D., and Spiegelman, B.M. (2006). Adipocytes as regulators of energy balance and
863 glucose homeostasis. Nature *444*, 847 853. 10.1038/nature05483.
864 2. Morigny, P., Boucher, J., Arner, P., and Langin, D. (2021). Lipid and glucose metabolism in
865 white adipocytes: pathways, dysfunction and therapeutics. Nat Rev Endocrinol *17*, 276–295.
866 10.1038/s41574-021-00471-8.
867 3. Grabner, G.F., Xie, H., Schweiger, M., and Zechner, R. (2021). Lipolysis: cellular mechanisms
868 for lipid mobilization from fat stores. Nat Metabolism *3*, 1445–1465. 10.1038/s42255-021-
869 00493-6.
870 4. Robbins, A.L., and Savage, D.B. (2015). The genetics of lipid storage and human
871 lipodystrophies. Trends Mol Med *21*, 1 6. 10.1016/j.molmed.2015.04.004.
872 5. Samuel, V.T., and Shulman, G.I. (2012). Mechanisms for Insulin Resistance: Common Threads
873 and Missing Links. Cell *148*, 852–871. 10.1016/j.cell.2012.02.017.
874 6. Guilherme, A., Virbasius, J.V., Puri, V., and Czech, M.P. (2008). Adipocyte dysfunctions linking
875 obesity to insulin resistance and type 2 diabetes. Nat Rev Mol Cell Bio *9*, 367 377.
876 10.1038/nrm2391.
877 7. Olzmann, J.A., and Carvalho, P. (2019). Dynamics and functions of lipid droplets. Nat Rev Mol
878 Cell Bio *20*, 137 155. 10.1038/s41580-018-0085-z.
879 8. Walther, T.C., Chung, J., and Farese, R.V. (2017). Lipid Droplet Biogenesis. Annu Rev Cell Dev
880 Bi *33*, 491–510. 10.1146/annurev-cellbio-100616-060608.
881 9. Pol, A., Gross, S.P., and Parton, R.G. (2014). Review: biogenesis of the multifunctional lipid
882 droplet: lipids, proteins, and sites. J Cell Biology *204*, 635 646. 10.1083/jcb.201311051.
883 10. Wolins, N.E., Quaynor, B.K., Skinner, J.R., Schoenfish, M.J., Tzekov, A., and Bickel, P.E.
884 (2005). S3-12, Adipophilin, and TIP47 package lipid in adipocytes. J Biol Chem *280*, 19146
885 19155. 10.1074/jbc.m500978200.
886 11. Wolins, N.E., Quaynor, B.K., Skinner, J.R., Tzekov, A., Croce, M.A., Gropler, M.C., Varma, V.,
887 Yao-Borengasser, A., Rasouli, N., Kern, P.A., et al. (2006). OXPAT/PAT-1 is a PPAR-induced lipid
888 droplet protein that promotes fatty acid utilization. Diabetes *55*, 3418 3428. 10.2337/db06-
889 0399.
890 12. Kassan, A., Herms, A., Fernández-Vidal, A., Bosch, M., Schieber, N.L., Reddy, B.J.N., Fajardo,
891 A., Gelabert-Baldrich, M., Tebar, F., Enrich, C., et al. (2013). Acyl-CoA synthetase 3 promotes
892 lipid droplet biogenesis in ER microdomains. J Cell Biology *203*, 985 1001.
893 10.1083/jcb.201305142.
894 13. Olarte, M.-J., Kim, S., Sharp, M.E., Swanson, J.M.J., Farese, R.V., and Walther, T.C. (2020).
895 Determinants of Endoplasmic Reticulum-to-Lipid Droplet Protein Targeting. Dev Cell.
896 10.1016/j.devcel.2020.07.001.
897 14. Dhiman, R., Caesar, S., Thiam, A.R., and Schrul, B. (2019). Mechanisms of protein targeting
898 to lipid droplets: A unified cell biological and biophysical perspective. Semin. cell Dev. Biol. *108*,
899 4–13. 10.1016/j.semcdb.2020.03.004.
900 15. Mathiowetz, A.J., and Olzmann, J.A. (2024). Lipid droplets and cellular lipid flux. Nat. Cell
901 Biol. *26*, 331–345. 10.1038/s41556-024-01364-4.
902 16. Wilfling, F., Wang, H., Haas, J.T., Krahmer, N., Gould, T.J., Uchida, A., Cheng, J.-X., Graham,
903 M., Christiano, R., Fröhlich, F., et al. (2013). Triacylglycerol synthesis enzymes mediate lipid

904 droplet growth by relocalizing from the ER to lipid droplets. Dev Cell *24*, 384 399.
905 10.1016/j.devcel.2013.01.013.
906 17. Eisenberg-Bord, M., Mari, M., Weill, U., Rosenfeld-Gur, E., Moldavski, O., Castro, I.G., Soni,
907 K.G., Harpaz, N., Levine, T.P., Futerman, A.H., et al. (2018). Identification of seipin-linked factors
908 that act as determinants of a lipid droplet subpopulation. J Cell Biol *217*, 269 282.
909 10.1083/jcb.201704122.
910 18. Chitraju, C., Mejhert, N., Haas, J.T., Diaz-Ramirez, L.G., Grueter, C.A., Imbriglio, J.E., Pinto, S.,
911 Koliwad, S.K., Walther, T.C., and Jr, R.V.F. (2017). Triglyceride Synthesis by DGAT1 Protects
912 Adipocytes from Lipid-Induced ER Stress during Lipolysis. Cell Metab *26*, 407 418.e3.
913 10.1016/j.cmet.2017.07.012.
914 19. Thiam, A.R., and Beller, M. (2017). The why, when and how of lipid droplet diversity. J Cell
915 Sci *130*, 315–324. 10.1242/jcs.192021.
916 20. Straub, B.K., Stoeffel, P., Heid, H., Zimbelmann, R., and Schirmacher, P. (2008). Differential
917 pattern of lipid droplet-associated proteins and de novo perilipin expression in hepatocyte
918 steatogenesis. Hepatology *47*, 1936–1946. 10.1002/hep.22268.
919 21. Hsieh, K., Lee, Y.K., Londos, C., Raaka, B.M., Dalen, K.T., and Kimmel, A.R. (2012). Perilipin
920 family members preferentially sequester to either triacylglycerol-specific or cholesteryl-ester-
921 specific intracellular lipid storage droplets. J Cell Sci *125*, 4067 4076. 10.1242/jcs.104943.
922 22. Herms, A., Bosch, M., Ariotti, N., Reddy, B.J.N., Fajardo, A., Fernández-Vidal, A., Alvarez-
923 Guaita, A., Fernández-Rojo, M.A., Rentero, C., Tebar, F., et al. (2013). Cell-to-cell heterogeneity
924 in lipid droplets suggests a mechanism to reduce lipotoxicity. Curr Biol *23*, 1489 1496.
925 10.1016/j.cub.2013.06.032.
926 23. Henne, M., Goodman, J.M., and Hariri, H. (2019). Spatial compartmentalization of lipid
927 droplet biogenesis. Biochimica Et Biophysica Acta Mol Cell Biology Lipids *1865*, 158499.
928 10.1016/j.bbalip.2019.07.008.
929 24. Ugrankar, R., Bowerman, J., Hariri, H., Chandra, M., Chen, K., Bossanyi, M.-F., Datta, S.,
930 Rogers, S., Eckert, K.M., Vale, G., et al. (2019). Drosophila Snazarus Regulates a Lipid Droplet
931 Population at Plasma Membrane-Droplet Contacts in Adipocytes. Dev Cell *50*, 557-572.e5.
932 10.1016/j.devcel.2019.07.021.
933 25. Heid, H., Rickelt, S., Zimbelmann, R., Winter, S., Schumacher, H., Dörflinger, Y., Kuhn, C., and
934 Franke, W.W. (2014). On the formation of lipid droplets in human adipocytes: the organization
935 of the perilipin-vimentin cortex. Plos One *9*, e90386. 10.1371/journal.pone.0090386.
936 26. Wolins, N.E., Brasaemle, D.L., and Bickel, P.E. (2006). A proposed model of fat packaging by
937 exchangeable lipid droplet proteins. Febs Lett *580*, 5484 5491. 10.1016/j.febslet.2006.08.040.
938 27. Freyre, C.A.C., Rauher, P.C., Ejsing, C.S., and Klemm, R.W. (2019). MIGA2 Links
939 Mitochondria, the ER, and Lipid Droplets and Promotes De Novo Lipogenesis in Adipocytes. Mol
940 Cell *76*, 811-825.e14. 10.1016/j.molcel.2019.09.011.
941 28. Kory, N., Farese, R.V., and Walther, T.C. (2016). Targeting Fat: Mechanisms of Protein
942 Localization to Lipid Droplets. Trends Cell Biol *26*. 10.1016/j.tcb.2016.02.007.
943 29. Olarte, M.-J., Swanson, J.M.J., Walther, T.C., and Farese, R.V. (2022). The CYTOLD and
944 ERTOLD pathways for lipid droplet–protein targeting. Trends Biochem. Sci. *47*, 39–51.
945 10.1016/j.tibs.2021.08.007.

946 30. Prévost, C., Sharp, M.E., Kory, N., Lin, Q., Voth, G.A., Farese, R.V., and Walther, T.C. (2018).
947 Mechanism and Determinants of Amphipathic Helix-Containing Protein Targeting to Lipid
948 Droplets. Dev Cell *44*, 73 86.e4. 10.1016/j.devcel.2017.12.011.
949 31. Kory, N., Thiam, A.-R., Farese, R.V., and Walther, T.C. (2015). Protein Crowding Is a
950 Determinant of Lipid Droplet Protein Composition. Dev Cell *34*, 351–363.
951 10.1016/j.devcel.2015.06.007.
952 32. Rowe, E.R., Mimmack, M.L., Barbosa, A.D., Haider, A., Isaac, I., Ouberai, M.M., Thiam, A.R.,
953 Patel, S., Saudek, V., Siniossoglou, S., et al. (2016). Conserved Amphipathic Helices Mediate
954 Lipid Droplet Targeting of Perilipins 1-3. J Biol Chem *291*, 6664 6678. 10.1074/jbc.m115.691048.
955 33. Čopič, A., Antoine-Bally, S., Giménez-Andrés, M., Garay, C.T., Antonny, B., Manni, M.M.,
956 Pagnotta, S., Guihot, J., and Jackson, C.L. (2018). A giant amphipathic helix from a perilipin that
957 is adapted for coating lipid droplets. Nat Commun *9*, 1 16. 10.1038/s41467-018-03717-8.
958 34. Giménez-Andrés, M., Emeršič, T., Antoine-Bally, S., D'Ambrosio, J.M., Antonny, B., Derganc,
959 J., and Čopič, A. (2021). Exceptional stability of a perilipin on lipid droplets depends on its polar
960 residues, suggesting multimeric assembly. Elife *10*, e61401. 10.7554/elife.61401.
961 35. Chorlay, A., Monticelli, L., Ferreira, J.V., M'barek, K.B., Ajjaji, D., Wang, S., Johnson, E., Beck,
962 R., Omrane, M., Beller, M., et al. (2019). Membrane Asymmetry Imposes Directionality on Lipid
963 Droplet Emergence from the ER. Dev Cell *50*, 25-42.e7. 10.1016/j.devcel.2019.05.003.
964 36. Bickel, P.E., Tansey, J.T., and Welte, M.A. (2009). PAT proteins, an ancient family of lipid
965 droplet proteins that regulate cellular lipid stores. Biochimica Et Biophysica Acta Bba - Mol Cell
966 Biology Lipids *1791*, 419 440. 10.1016/j.bbalip.2009.04.002.
967 37. Londos, C., Brasaemle, D.L., Schultz, C.J., Segrest, J.P., and Kimmel, A.R. (1999). Perilipins,
968 ADRP, and other proteins that associate with intracellular neutral lipid droplets in animal cells.
969 Semin Cell Dev Biol *10*, 51 58. 10.1006/scdb.1998.0275.
970 38. Kimmel, A.R., and Sztalryd, C. (2016). The Perilipins: Major Cytosolic Lipid Droplet–
971 Associated Proteins and Their Roles in Cellular Lipid Storage, Mobilization, and Systemic
972 Homeostasis*. Annu Rev Nutr *36*, 471 509. 10.1146/annurev-nutr-071813-105410.
973 39. Brasaemle, D.L. (2007). Thematic review series: adipocyte biology. The perilipin family of
974 structural lipid droplet proteins: stabilization of lipid droplets and control of lipolysis. J Lipid Res
975 *48*, 2547 2559. 10.1194/jlr.r700014-jlr200.
976 40. Garcia, A., Subramanian, V., Sekowski, A., Bhattacharyya, S., Love, M.W., and Brasaemle,
977 D.L. (2004). The amino and carboxyl termini of perilipin a facilitate the storage of
978 triacylglycerols. J Biol Chem *279*, 8409 8416. 10.1074/jbc.m311198200.
979 41. Choi, Y.M., Ajjaji, D., Fleming, K.D., Borbat, P.P., Jenkins, M.L., Moeller, B.E., Fernando, S.,
980 Bhatia, S.R., Freed, J.H., Burke, J.E., et al. (2023). Structural insights into perilipin 3 membrane
981 association in response to diacylglycerol accumulation. Nat. Commun. *14*, 3204.
982 10.1038/s41467-023-38725-w.
983 42. Garcia, A., Sekowski, A., Subramanian, V., and Brasaemle, D.L. (2003). The central domain is
984 required to target and anchor perilipin A to lipid droplets. J Biol Chem *278*, 625 635.
985 10.1074/jbc.m206602200.
986 43. Ajjaji, D., M'barek, K.B., Mimmack, M.L., England, C., Herscovitz, H., Dong, L., Kay, R.G.,
987 Patel, S., Saudek, V., Small, D.M., et al. (2019). Dual binding motifs underpin the hierarchical
988 association of perilipins1–3 with lipid droplets. Mol Biol Cell *30*, 703–716. 10.1091/mbc.e18-08-
989 0534.

990 44. Wolins, N.E., Skinner, J.R., Schoenfish, M.J., Tzekov, A., Bensch, K.G., and Bickel, P.E. (2003).
991 Adipocyte protein S3-12 coats nascent lipid droplets. J Biol Chem *278*, 37713 37721.
992 10.1074/jbc.m304025200.
993 45. Skinner, J.R., Harris, L.-A.L.S., Shew, T.M., Abumrad, N.A., and Wolins, N.E. (2013). Perilipin 1
994 moves between the fat droplet and the endoplasmic reticulum. Adipocyte *2*, 80 86.
995 10.4161/adip.22864.
996 46. Shibata, Y., Hu, J., Kozlov, M.M., and Rapoport, T.A. (2009). Mechanisms shaping the
997 membranes of cellular organelles. Annu Rev Cell Dev Bi *25*, 329 354.
998 10.1146/annurev.cellbio.042308.113324.
999 47. Parton, R.G., and Pozo, M.A. del (2013). Caveolae as plasma membrane sensors, protectors
1000 and organizers. Nat Rev Mol Cell Bio *14*, 98 112. 10.1038/nrm3512.
1001 48. Schrul, B., and Kopito, R.R. (2016). Peroxin-dependent targeting of a lipid-droplet-destined
1002 membrane protein to ER subdomains. Nat Cell Biol *18*, 1 26. 10.1038/ncb3373.
1003 49. Caillon, L., Nieto, V., Gehan, P., Omrane, M., Rodriguez, N., Monticelli, L., and Thiam, A.R.
1004 (2020). Triacylglycerols sequester monotopic membrane proteins to lipid droplets. Nat
1005 Commun *11*, 3944. 10.1038/s41467-020-17585-8.
1006 50. Wilfling, F., Thiam, A.R., Olarte, M.-J., Wang, J., Beck, R., Gould, T.J., Allgeyer, E.S., Pincet, F.,
1007 Bewersdorf, J., Farese, R.V., et al. (2014). Arf1/COPI machinery acts directly on lipid droplets
1008 and enables their connection to the ER for protein targeting. Elife *3*, e01607.
1009 10.7554/elife.01607.
1010 51. Song, J., Mizrak, A., Lee, C.-W., Cicconet, M., Lai, Z.W., Tang, W.-C., Lu, C.-H., Mohr, S.E.,
1011 Farese, R.V., and Walther, T.C. (2022). Identification of two pathways mediating protein
1012 targeting from ER to lipid droplets. Nat Cell Biol, 1–14. 10.1038/s41556-022-00974-0.
1013 52. Xu, D., Li, Y., Wu, L., Li, Y., Zhao, D., Yu, J., Huang, T., Ferguson, C., Parton, R.G., Yang, H., et
1014 al. (2018). Rab18 promotes lipid droplet (LD) growth by tethering the ER to LDs through SNARE
1015 and NRZ interactions. J. Cell Biol. *217*, 975–995. 10.1083/jcb.201704184.
1016 53. Mann, J.P., and Savage, D.B. (2019). What lipodystrophies teach us about the metabolic
1017 syndrome. J Clin Invest *129*, 4009–4021. 10.1172/jci129190.
1018 54. Tansey, J.T., Sztalryd, C., Gruia-Gray, J., Roush, D.L., Zee, J.V., Gavrilova, O., Reitman, M.L.,
1019 Deng, C.-X., Li, C., Kimmel, A.R., et al. (2001). Perilipin ablation results in a lean mouse with
1020 aberrant adipocyte lipolysis, enhanced leptin production, and resistance to diet-induced
1021 obesity. Proc. Natl. Acad. Sci. *98*, 6494–6499. 10.1073/pnas.101042998.
1022 55. Gandotra, S., Lim, K., Girousse, A., Saudek, V., O'Rahilly, S., and Savage, D.B. (2011). Human
1023 frame shift mutations affecting the carboxyl terminus of perilipin increase lipolysis by failing to
1024 sequester the adipose triglyceride lipase (ATGL) coactivator AB-hydrolase-containing 5
1025 (ABHD5). J Biological Chem *286*, 34998–35006. 10.1074/jbc.m111.278853.
1026 56. Garg, A. (2011). Clinical review#: Lipodystrophies: genetic and acquired body fat disorders. J
1027 Clin Endocrinol Metabolism *96*, 3313 3325. 10.1210/jc.2011-1159.
1028 57. Melvin, A., Stears, A., and Savage, D.B. (2019). Recent developments in lipodystrophy. Curr.
1029 Opin. Lipidol. *30*, 284–290. 10.1097/mol.0000000000000613.
1030 58. Koprulu, M., Zhao, Y., Wheeler, E., Dong, L., Rocha, N., Li, C., Griffin, J.D., Patel, S., Streek,
1031 M.V. de, Glastonbury, C.A., et al. (2021). Identification of rare loss of function genetic variation
1032 regulating body fat distribution. J. Clin. Endocrinol. Metab. *107*, dgab877-.
1033 10.1210/clinem/dgab877.

1034 59. Patel, K.A., Burman, S., Laver, T.W., Hattersley, A.T., Frayling, T.M., and Weedon, M.N.
1035 (2022). PLIN1 Haploinsufficiency Causes a Favorable Metabolic Profile. J. Clin. Endocrinol.
1036 Metab. *107*, e2318–e2323. 10.1210/clinem/dgac104.
1037 60. Rapoport, T.A., Li, L., and Park, E. (2016). Structural and Mechanistic Insights into Protein
1038 Translocation. Annu. Rev. Cell Dev. Biol. *33*, 1–22. 10.1146/annurev-cellbio-100616-060439.
1039 61. Hegde, R.S., and Keenan, R.J. (2022). The mechanisms of integral membrane protein
1040 biogenesis. Nat. Rev. Mol. Cell Biol. *23*, 107–124. 10.1038/s41580-021-00413-2.
1041 62. Krogh, A., Larsson, B., Heijne, G. von, and Sonnhammer, E.L. (2001). Predicting
1042 transmembrane protein topology with a hidden Markov model: application to complete
1043 genomes. J Mol Biol *305*, 567 580. 10.1006/jmbi.2000.4315.
1044 63. Jayasinghe, S., Hristova, K., and White, S.H. (2001). Energetics, stability, and prediction of
1045 transmembrane helices. J Mol Biol *312*, 927 934. 10.1006/jmbi.2001.5008.
1046